# A persistent giant algal virus, with a unique morphology, encodes an unprecedented number of genes involved in energy metabolism

Romain Blanc-Mathieu[1,2], Håkon Dahle[3], Antje Hofgaard[4], David Brandt[5], Hiroki Ban[1], Jörn Kalinowski[5], Hiroyuki Ogata[1] and Ruth-Anne Sandaa[6*]

1: Institute for Chemical Research, Kyoto University, Gokasho, Uji, 611-0011, Japan

2: Laboratoire de Physiologie Cellulaire & Végétale, CEA, Univ. Grenoble Alpes, CNRS, INRA, IRIG, Grenoble, France

3: Department of Biological Sciences and K.G. Jebsen Center for Deep Sea Research, University of Bergen, Bergen, Norway

4: Department of Biosciences, University of Oslo, Norway

5: Center for Biotechnology, Universität Bielefeld, Bielefeld, 33615, Germany

6: Department of Biological Sciences, University of Bergen, Bergen, Norway

*Corresponding author: Ruth-Anne Sandaa, +47 55584646, ruth.sandaa@uib.no

# Abstract

Viruses have long been viewed as entities possessing extremely limited metabolic capacities. Over the last decade, however, this view has been challenged, as metabolic genes have been identified in viruses possessing large genomes and virions—the synthesis of which is energetically demanding. Here, we unveil peculiar phenotypic and genomic features of *Prymnesium kappa* virus RF01 (PkV RF01), a giant virus of the *Mimiviridae* family. We found that this virus encodes an unprecedented number of proteins involved in energy metabolism, such as all four succinate dehydrogenase (SDH) subunits (A–D) as well as key enzymes in the *β*-oxidation pathway. The *SDHA* gene was transcribed upon infection, indicating that the viral SDH is actively used by the virus— potentially to modulate its host's energy metabolism. We detected orthologous *SDHA* and *SDHB* genes in numerous genome fragments from uncultivated marine *Mimiviridae* viruses, which suggests that the viral SDH is widespread in oceans. PkV RF01 was less virulent compared with other cultured prymnesioviruses, a phenomenon possibly linked to the metabolic capacity of this virus and suggestive of relatively long co-evolution with its hosts. It also has a unique morphology, compared to other characterized viruses in the *Mimiviridae* family. Finally, we found that PkV RF01 is the only alga-infecting *Mimiviridae* virus encoding two aminoacyl-tRNA synthetases and enzymes corresponding to an entire base-excision repair pathway, as seen in heterotroph-infecting *Mimiviridae*. These *Mimiviridae* encoded-enzymes were found to be monophyletic and branching at the root of the eukaryotic tree of life. This placement suggests that the last common ancestor of *Mimiviridae* was endowed with a large, complex genome prior to the divergence of known extant eukaryotes.

## Importance

Viruses on Earth are tremendously diverse in terms of morphology, functionality, and genomic composition. Over the last decade, the conceptual gap separating viruses and cellular life has tightened because of the detection of metabolic genes in viral genomes that express complex virus phenotypes upon infection. Here, we describe *Prymnesium kappa* virus RF01, a large alga-infecting virus with a unique morphology, an atypical infection profile, and an unprecedented number of genes involved in energy metabolism (such as the tricarboxylic (TCA) cycle and the *β*-oxidation pathway). Moreover, we show that the gene corresponding to one of these enzymes (the succinate dehydrogenase subunit A) is transcribed during infection and is widespread among marine viruses. This discovery provides evidence that a virus has the potential to actively regulate energy metabolism with its own gene.

**Key words**: algal viruses, *Mimiviridae*, persistent, co-evolution, metabolism, energy production, succinate dehydrogenase, *β*-oxidation and aminoacyl-tRNA synthetases

# Introduction

In their essay "Varieties of Living Things: Life at the Intersection of Lineage and Metabolism," Dupré and O'Malley proposed to address Schrödinger's question "What is Life?" by "*describing a spectrum of biological entities that illustrates why no sharp dividing line between living and non-living things is likely to be useful*" (1). Microbiologists have contributed considerably to this descriptive effort, both by reporting the existence of viruses endowed with genes coding for functions once thought to be exclusive to cellular life and by concomitantly proposing that actively infecting viruses are a "living form" (2–4). Genes encoding elements for photosynthesis (5, 6), carbon metabolism (7), and nitrogen- (8) and sulfur-cycling (9) have been found in bacterial viruses, where they are used to maintain or augment cellular processes during infection and to redirect energy and resources towards viral production (8, 10, 11). Genes for protein synthesis, including translation initiation, elongation, and termination, and a range of aminoacyl-tRNA synthetases have been found in *Mimiviridae*, a group of giant viruses infecting single-celled eukaryotes (12–14). *Mimiviridae* and other large DNA viruses, including some bacterial viruses, also have tRNA genes (15, 16). Ribosomal proteins have recently been reported in viral genomes derived from metagenomes (17). Genes involved in other metabolic processes, such as fermentation (18), glycosylation (19), photosynthesis (20), and rhodopsin (21), are encoded in *Mimiviridae* and other related large eukaryotic DNA viruses. Metabolic genes are frequently observed within virus genomes (20, 22, 23); although they represent a tiny fraction of the viral gene pool, these genes have the potential to dramatically modify the phenotype of an actively infected cell and alter the ecological role of the host (7, 24, 25). The infected host in this state has been referred to as a virocell (2). One might expect that the interplay between viral genes

and host genes in virocells would become increasingly fine-tuned and complex during prolonged virus–host co-evolution, which also typically leads to lower virulence. Much of the complexity of virocells may still be undetected, as most *Mimiviridae* isolated with their natural host (mostly algae) are highly virulent, with several involved in rapid algal bloom termination events (26).

Viruses of the *Mimiviridae* family are known to infect heterotrophic and autotrophic microbial eukaryotes. This divide is also reflected in the phylogeny of these viruses, some of which are classified into two proposed sub-families: "Megavirinae" and "Mesomimivirinae" (27). The former contains viruses with genomes larger than 1 Mbp, all isolated from Amoebozoa, while the latter includes viruses with smaller genomes isolated from haptophyte algae of class Prymnesiophyceae. Several *Mimiviridae* members outside these two groups have been characterized to some extent as well, namely, viruses isolated from heterotrophs (*Cafeteria roenbergensis* virus, CroV; *Bodo saltans* virus, BsV; Choano virus), autotrophs (*Aureococcus anophagefferens* virus, AaV; Tetraselmis virus 1, TetV; *Pyramimonas orientalis* virus, PoV; *Prymnesium kappa* virus RF01, PkV RF01), a metazoan (Namao virus), and metagenomes (Klosneuviruses). The Mesomimivirinae sub-family includes viruses infecting bloom-forming hosts, such as *Phaeocystis pouchetii*, *Phaeocystis globosa*, and *Prymnesium parvum* (PpV, PgV Group I, and PpDVAV, respectively) (28–30); it also includes several viruses infecting *Haptolina ericina* and *Prymnesium kappa*, which normally do not form massive blooms but are present at low densities in seawater year round (31). In marine environments, viruses infecting low-density and non-bloom-forming algae may be the most common virus–host systems—that is, low-density hosts (non-blooming) and viruses that appear to have co-evolved in response to host growth strategy. Thus far, the only known

representatives of such viruses are *Prymnesium kappa* viruses RF01 (PkV RF01) and RF02 (PkV RF02), *Haptolina ericina* virus RF02 (HeV RF02), and *Chrysochromulina ericina* virus (CeV 01B, infecting *Haptolina ericina*) (32, 33). Together with PgV, all of these viruses, except for PkV RF01, belong to the sub-family Mesomimivirinae on the basis of their monophyletic relationship and, in the case of PgV and CeV, a shared genomic similarity (27). In contrast, phylogenetic analysis of two partially sequenced marker genes has placed PkV RF01 deep inside the *Mimiviridae* clade, and characterization of its life cycle has revealed an atypical infection profile (33). Here, we report new phenotypic features as well as new viral functions inferred from analysis of the genome sequence of PkV RF01. We found that this virus has a unique morphology, is less virulent than most other alga-infecting viruses and possesses an unprecedented number of energy-generating genes. We uncovered clues suggesting that members of *Mimiviridae* that potentially modulate the metabolism of their hosts are widespread in the ocean. Our findings of peculiar genomic features in a persistent virus provide new insights on virus–host coevolution and may stimulate further advances in modeling the history of their interaction.

# Results and Discussion

## PkV RF01 has an atypical morphology

The icosahedral PkV RF01 particle is approximately 400 nm in diameter (Fig. 1A-B). Beneath the capsid, several convoluted inner membranes fill approximately 66% of the interior. Treatment of chloroform can be used to identify possible functions of lipid membranes, as it acts to remove lipid molecules that might be essential for successful infection (34). Some algal viruses in the NCLDV group are sensitive to chloroform (30, 35, 36) with the suggestions that lipid containing inner or outer

membranes are involved in the infection process (35, 37). In our experiment, chloroform treatment of PkV RF01 drastically reduced the infectivity of the virus. (Fig. 1C). As no outer membrane was detected by cryo-electron tomography, the sensitivity to chloroform might be linked to lipid components in either the capsid or the inner convoluted membranes. Internal lipid-containing membranes have been detected in several icosahedral-shaped double-stranded DNA viruses, including algal viruses belonging to families *Phycodnaviridae* and *Mimiviridae*, mimiviruses, and various bacteriophages (38–43). In all of these viruses, the inner membranes are suggested to play a role in the release of the viral nucleoprotein core or genome by fusing with the host plasma membrane (40, 42, 43). Inner membranes in currently described NCLDVs more or less adopt the icosahedral morphology defined by the outer layer of capsomers (44, 45). We detected several convoluted inner membranes in PkV RF01 that do not follow the structure of the capsid. To our knowledge, this structural inconsistency has not been previously detected in any double-stranded DNA viruses, which calls for further investigation to understand the assembly process of PkV RF01 and how it enters its host. Another striking feature of the PkV RF01 virion is an internal rod-shaped core (ca. 55 nm in diameter), which is filled with dense material and positioned in the center of the virus particle. Similar features have been observed in TEM images of large virus-like particles (VLPs) (300–700 nm) occurring in waste vacuoles of phaeodarian radiolarians collected from different oceans (46) and in zoospores of the green alga *Chlorococcus minutum* (47). To our knowledge, however, these features have not been described in isolated viruses thus far.

## PkV RF01 has an atypical infection strategy

Only 2% of the total PkV RF01 viral particles produced during infection of *Haptolina ericina* UiO028 (He UiO028) were infectious (able to produce progeny) (Table 1). This infectivity was much lower than that of the other two prymnesioviruses, HeV RF02 and PkV RF02, which produced 13% and 44% of infectious progeny respectively (Table 1). The portion of infectious particles of PkV RF01 is low also when compared to other algal viruses (48, 49). In addition, the latent period of PkV RF01 was previously reported to be longer (ca. 24–32 h, (33)) in comparison with other prymnesioviruses (28, 29, 32, 33) and it has been demonstrated that PkV RF01 is also able to infect multi-species (33), that is another unusual trait among algal viruses (26).

The hosts of PkV RF01, PkV RF02, and HeV RF02 all belong to order the Prymnesiales, whose members are normally present in low abundance but co-occur year round (*K*-strategists) (50). PkV RF01, PkV RF02, and HeV RF02 are less virulent, as shown in the present study, and have longer latent periods compared with viruses infecting bloom-forming haptophytes (*r*-strategists). Two of these viruses (PkV RF01 and HeV RF02) are also able to infect multi species (generalists) (33). Longer replication time and reduced virulence, as hosts becomes scarce, increases the chances of vertical transmission rather than horizontal transmission of a virus. As vertical parent-to-offspring transmission depends on host reproduction, it has been argued that such transmission should select for reduced virulence because the virus depend on host survival and reproduction for its transmission (51, 52). High virulence, on the other hand, may be supported by large, dense host populations, as e.g. algal blooms, because high host densities ensure successful horizontal transmission of viral progeny to new hosts (51, 53). Viruses infecting the recurrent

bloom-forming haptophytes, *Phaeocystis pouchetii* virus (PpV), and *Phaeocystis globosa* virus (PgV), are indeed highly virulent with between 60%–100% of virus particles produced being infectious, resulting in rapid lysis of their hosts (48, 54). Broad host range might also increase the chance of transmission in an environment with low host abundances (*K*-strategists). Such strategy requires a tradeoff whereby the virus decreases its opportunity of transmission by evolving longer replication times, higher decay rates and reduced infectivity (discussed in (55, 56)). This fits well with our two multi-species infecting haptophyte viruses, PkV RF01 and HeV RF02, that have reduced proportions of infectious particles and longer replication times (33), relative to other haptophyte viruses with restricted host ranges (specialists) like e.g. the *Emiliania huxleyi* virus (EhV), PpV and PgV.

The balance between fitness traits, such as virulence, latent period and host range, and tradeoffs is the result of the adaptive evolution between viruses and their hosts, resulting in relationships spanning from acute to stable coexistence (persistence). In the ocean, persistent relationships—such as between PkV RF01 and its hosts—seem to be most common among viruses infecting unicellular algae; this has been demonstrated by several metabarcoding studies revealing the persistence of dominance of viral OTUs over several months (57, 58). The atypical infection strategy of PkV RF01 evokes a persistent nature, different than the vast majority of other so far characterized algal viruses.

## PkV RF01 has the largest genome among algal viruses

The genome of PkV RF01 was assembled as a linear DNA sequence of 1,421,182 bp. This size is more than twice that of the genome of TetV, which means that PkV RF01 has the largest reported genome of any virus infecting a photosynthetic organism (Fig. 2A). Evidence for the linear structure of this genome is the presence of ~5-kbp

terminal inverted repeats. Despite being phylogenetically more closely related to alga-infecting *Mimiviridae*, the genome size of PkV RF01 is in the range of heterotroph-infecting *Mimiviridae*. The overall G+C content of PkV RF01 is 22.8%, which is low compared with other *Mimiviridae* (23%–41%). Similar to other *Mimiviridae*, the average G+C content of PkV RF01 in intergenic regions is relatively low, 17.8%. This lower G+C content may reflect an ongoing loss of G and C nucleotides, more prevalent in non-coding than coding regions because of weaker background selection in non-coding regions. The genome of PkV RF01 is predicted to contain 1,161 genes comprising 1,121 protein-coding DNA sequences (CDSs) and 40 tRNA genes corresponding to 13 amino acids. Most tRNA genes (30 out of 40) are clustered in three genomic regions that lack predicted CDSs, a feature also observed in other *Mimiviridae*. For example, all tRNAs of TetV ($n$ = 10) and CroV ($n$ = 22) are encoded consecutively on the same strand (18, 59). The average CDS length is 1,046 bp (minimum: 297; maximum: 1,493). Intergenic regions average 217 bp in length, with a cumulative sum of 244,005 bp, which corresponds to a gene density of 82.8%.

Of the 1,121 predicted CDSs, 641 (57%) exhibited sequence similarities (BLASTP $E$-value conservative cutoff of $1 \times 10^{-5}$) to protein sequences in the UniRef90 database (Fig. 2A). Among them, 165 were most similar to *Mimiviridae*. Curiously, among the CDSs most similar to *Mimiviridae*, sixty were closest to ChoanoVirus which was isolated from choanoflagellates cultures, followed by Mesomimivirinae ($n$ = 49) and Klosneuvirinae ($n$ = 30) (Fig. 2B). Among the 181 closest homologs found in eukaryotic organisms 23 were haptophytes. A sequence-based homology search of corrected nanopore reads and scaffolds composing the initial assembly against *Lavidaviridae* proteomes (BLASTX; matrix: BLOSUM45, $E$-value $< 1 \times 10^{-5}$) yielded no significant alignments against any major or minor

*Lavidaviridae* capsid proteins, which suggests that virophages were absent from the sample used for sequencing.

A previous analysis of PkV RF01 family-B DNA polymerase (PolB) and the major capsid protein (MCP) placed this virus in the family *Mimiviridae* (33). We also recently reported that the PkV RF01 genome has additional NCLDV core genes, such as A32-like virion packing ATPase (NCVOG0249) and RNApol (RNA pol subunit I [NCVOG0274] and subunit II [NCVOG0271]), and orthologous genes that are specific to *Mimiviridae,* namely, MutS7 (NCVOG2626) and asparagine synthase (AsnS, NCVOG0061) (60). Phylogenetic reconstruction using five NCLDV core genes confirmed the deep branching of PkV RF01 within the *Mimiviridae* family and suggested that PkV RF01, along with ChoanoV1, TetV and AaV, is more closely related to Mesomimivirinae than to Megavirinae (Fig. 3A). In support of this evolutionary relationship, PkV RF01 has an additional copy of the second largest RNA polymerase subunit gene (*rpb2*). This *rpb2* duplication is shared with all other *Mimiviridae* infecting algae, including Mesomimivirinae members, AaV (whose second copy is very short), and TetV and was previously proposed as a useful feature to discriminate between the two main clades (autotroph versus heterotroph-infecting viruses) within the *Mimiviridae* family (27). This additional *rpb2* copy is not found in other *Mimiviridae* to the exception of ChoanoV1 whose genome was derived from a single cell metagenome in choanoflagellates cultures. Phylogenetic analysis indicates that these two *rbp2* copies were present in the ancestor of alga-infecting *Mimiviridae* and ChoanoV1 (Fig. 3B). In agreement with the five NCLDV core genes phylogeny, it suggests that PkV RF01 and ChoanoV1, although evolutionarily distant, are more related with each other compared to any other *Mimiviridae*.

Out of 1,121 predicted protein-coding genes in the genome of PkV RF01, only about a third could be annotated with some functional description based on their sequence homology with characterized proteins. Such a small percentage is typical of divergent eukaryotic viruses detected for the first time. A total of 339 proteins (30%) showed significant sequence similarity with proteins in the Cluster of Orthologous Gene (COG) database (61) (Fig. 4). The distribution of COG functions associated with these hits was dominated by "Posttranslational modification, protein turnover, chaperones" (43 proteins) and "Cell wall/membrane/envelope biogenesis" (42 proteins), which is approximately two times more proteins than in other *Mimiviridae* members except for Tupanvirus. Among other well-represented categories, numbers of proteins in "Replication, recombination and repair" (36 proteins) and "Transcription" (23 proteins) were similar to those of other *Mimiviridae*, while the categories of "Translation, ribosomal structure and biogenesis" (25 proteins) and "Amino acid transport and metabolism" (20 proteins) were respectively in the same range or higher than those of heterotroph-infecting *Mimiviridae* (mimiviruses, BsV, and CroV). Interestingly, 24, 17, and 9 PkV RF01 proteins were respectively assigned to the categories of "Lipid transport and metabolism", "Carbohydrates transport and metabolism," and "Energy production and conservation," all much higher compared with other *Mimiviridae* viruses (Fig. 5).

Similar to other *Mimiviridae*, PkV RF01 encodes several genes involved in DNA repair, transcription, and translation. Notably, this virus has the full set of enzymes required for the base excision repair (BER) pathway, which is also the case for all *Mimiviridae* members except for those with smaller genomes (PgV, CeV, and AaV). PkV RF01 BER enzymes are closer (i.e., have a greater alignment score) to heterotroph-infecting *Mimiviridae* than to cellular homologs, thus suggesting that this

pathway was present in the last common ancestor of *Mimiviridae*. According to a previous phylogenetic analysis, *Mimiviridae* BER enzymes are monophyletic with regard to *Mimiviridae* and have not recently been acquired from eukaryotes (62).

Unlike alga-infecting *Mimiviridae*, PkV RF01 encodes two amino-acyl tRNA synthetases (aaRS): an isoleucyl-tRNA synthetase (IleRS; ORF 480) and an asparaginyl-tRNA synthetase (AsnRS; ORF 764). Both of these synthetases are found in most lineages of heterotroph-infecting *Mimiviridae* (AsnRS is missing from CroV and BsV, and IleRS is missing from *Mimivirus* lineage A). Phylogenetic analyses of these two proteins revealed a deep branching of viral homologs, which formed a monophyletic clade well separated from cellular homologs (Fig. 6).

## A viral-encoded succinate dehydrogenase and energy production genes

We found six predicted protein-coding genes (ORFs 893 to 900) related to energy production in an 8,026-bp region (Fig. 7A). Four ORFs (ORFs 893 and 898–900) were predicted to code for all four subunits (SDHA, D, C, and B) of a functional succinate dehydrogenase (SDH, or Electron Transport Chain Complex II) of the oxidative phosphorylation pathway (Fig. 7B). In eukaryotes, all four subunits of this enzyme are encoded in the nuclear genome. This enzyme acts in the mitochondrial respiratory chain and participates in both the TCA cycle and the respiratory electron transfer chain. In the TCA cycle, this succinate dehydrogenase oxidizes succinate to fumarate, while its activity in the inner mitochondrial membrane involves the reduction of a FAD cofactor followed by electron transfer through three Fe–S centers to ubiquinone (Fig. 7C).

*SDH* genes have recently been reported in viral genomes assembled from environmental samples for which functional experiments cannot be done (63). In a RT-PCR experiment using primers specific for the PkV RF01 gene for SDHA

(hereafter, *vSDHA*), we detected transcripts of this gene in samples collected 24, 72, and 96 h post infection (Fig. 8). The *vSDHA* primers were tested on an uninfected culture to ensure that only the viral version of the *SDHA* gene was amplified (Fig. 9). The MCP gene of PkV RF01 was used both for protocol optimization and later as an internal positive control (Fig. 10). Although the transcription of the viral *SDHA* suggests that the viral SDH is functional, we can only speculate on the possible role of this enzyme during infection. One possibility is that the viral SDH sustains the carbohydrate metabolism of infected cells (i.e., virocells) to supply building blocks of viral particles such as amino acids and to support proper replication of this large virus. Another possibility is that PkV RF01 uses its SDH as a part of an arms race with its host to turn on the TCA cycle after the host had turned it off to counter viral replication, or more simply to boost the energy metabolism of the virocells to augment the fitness of the host and/or to maximize virus production efficiency.

The discovery of the viral SDH prompted us to search for other potential viral-encoded SDHA and SDHB homologs in marine metagenomes. These two subunits (SDHA and SDHB) form the catalytic core containing the redox cofactors that participate in electron transfer to ubiquinone; they are thus more conserved than SDHC and SDHD subunits. To test for the presence of this viral SDH in other viruses, we searched for *vSDHA* and *B* in marine metagenomes of the *Tara* Oceans expedition. The 50 most-similar and non-redundant SDHA and B sequences predicted from 101 *Tara* Oceans genome fragments were most likely derived from *Mimiviridae* viruses (Fig. 11). Indeed, out of 1,113 genes predicted from these 101 genome fragments, 681 were annotated at some taxonomic level, of which 449 were predicted to be cellular and 157 viral. Of the 157 viral genes, 146 and 130 had their last common ancestor in *Mimiviridae* and Mesomimivirinae, respectively. A total of 32 of

the 101-genome fragments contained at least one gene predicted to be of *Mimiviridae* origin, and the larger the genome fragment, the more *Mimiviridae* genes it was found to encode (Fig. 11A). Functional analysis indicated that 12 of the 1,113 predicted genes were NCLDV hallmark genes (encoding five VLTF3s, two capsid proteins, two PCNAs, two helicases, and one PolB). The high proportion of unknown genes and genes annotated as *Mimiviridae* in the 101 *Tara* Oceans genome fragments encoding SDHA or SDHB strongly suggests that these fragments belong to *Mimiviridae* viruses. This finding demonstrates that the presence of SDH is not restricted to PkV RF01 and is arguably widespread among marine *Mimiviridae*. According to phylogenetic analyses of cellular and viral SDHA and SDHB, the viral homologs form a monophyletic group that branches deeply within eukaryotic lineages (Fig. 11B-C). Long-branch attraction bias could generate such topologies but, as explained above for the IleRS and AsnRS, it is more likely that the viral SDHA and SDHB were acquired at an early stage in the radiation of eukaryotic lineages. The transcription of *vSDHA* and its occurrence in marine environments calls for further investigation to understand the biological role and co-evolutionary significance of this viral SDH.

Other genes related to energy production were detected in the 8,026 bp-long region. ORF 894 and ORF 896, respectively corresponding to cytochrome *c* (CytC) and cytochrome b6-f complex iron-sulfur (Cyt b6-f) subunits, showed high sequence conservation with *Chrysochromulina* sp. CCMP291 proteins (78% and 59% amino acid [aa] identities, respectively). CytC is a short protein (~100 aa) involved in the oxidative phosphorylation pathway, where it accommodates the transfer of electrons between the coenzymes Q-cytochrome *c* reductase (complex III) and cytochrome *c* oxidase (complex IV). The presence of Cyt b6-f between oxidative phosphorylation genes is puzzling because the cytochrome b6-f complex is involved in photosynthesis.

The core of the chloroplast b6f complex, however, is similar to the analogous respiratory cytochrome bc(1) complex. The other two predicted ORFs in this region are similar to ubiquinone biosynthesis protein UbiB (ORF 895) or contain a NAD-binding domain and a Fe-S cluster (ORF 897) and may thus be associated with electron transport as well. ORF 897 has two distant (25%–31% aa identity) homologs in the PkV RF01 genome (ORF 456 and ORF 625).

Some other genes were predicted to encode enzymes involved in pyruvate metabolism. ORF 79 has sequence homology with L-lactate dehydrogenases; it might thus catalyze the conversion of lactate to pyruvate, an intermediary compound serving as a starting point for several major metabolic pathways, such as glycolysis, gluconeogenesis, and the TCA cycle. ORF 727 was predicted to code for an isochorismate hydrolase that also produces pyruvate from isochorismate. ORF 24 and ORF 726 share sequence homology with phosphoenolpyruvate synthase and a partial pyruvate kinase, respectively. The former catalyzes the conversion of pyruvate to phosphoenolpyruvate (PEP), while the latter catalyzes the reverse reaction. Formation of PEP is an initial step in gluconeogenesis.

## A nearly complete viral-encoded β-oxidation pathway

In this study, 22 predicted genes were inferred to code for proteins involved in lipid synthesis or degradation, including key enzymes of the *β*-oxidation pathway (Table 2). Several genes were predicted to code for lipase-like proteins (ORFs 386, 481, 635, 653, and 690), including a triacylglycerol lipase (ORF 386) that can break down triacylglycerol into glycerol and fatty acids. Glycerol and fatty acids can be used as a starting point for ATP production—by glycolysis and *β*-oxidation, respectively. In the *β*-oxidation pathway, fatty acids are fully oxidized to produce acetyl-CoA, which can then enter the TCA cycle to yield NADH and FADH2; these latter two products can

376 funnel through to the electron transport chain to produce ATP (Fig. 7C). Each *β*-
377 oxidation cycle itself also produces NADH and FADH2 cofactors. We found that PkV
378 RF01 encodes key *β*-oxidation enzymes. First, two distantly related ORFs (ORF 142
379 and ORF 904 sharing 22% aa identity) have sequence homology with a long-chain
380 fatty acyl-CoA synthetase. This enzyme catalyzes the formation of fatty acyl-CoA in
381 the cytosol. Fatty acyl-CoA can be imported to mitochondria using a (carnitine) CoA-
382 transferase also encoded in PkV RF01 (ORF 33). Once in the mitochondrial matrix,
383 fatty acyl-CoA serves as a substrate on which an acyl-CoA dehydrogenase (ORF
384 1046) oxidizes the fatty acyl-CoA and reduces a FAD cofactor to produce a FADH2
385 cofactor. We identified a 2,4-dienoyl-CoA reductase (ORF 30) that may facilitate the
386 next oxidation step to produce a NADH cofactor. FADH2 and NADH molecules
387 produced by a *β*-oxidation cycle can both be oxidized in the electron transport chain
388 to generate ATP. The enzymes involved in the two intermediate steps following each
389 oxidation, either an enoyl-CoA hydratase or a β-ketothiolase, were not detected in our
390 analysis.

391 Most of these genes have no homologs in reference viral genomes, and, to our
392 knowledge, this is the first report of a virus possessing proteins directly involved in
393 lipid-based energy production. By diverting host lipid machinery, interactions of
394 viruses with lipids or lipid based-structures have long been known to have structural
395 or signaling roles at different stages of the virus life cycle, such as entry, genome
396 replication, morphogenesis, and exit (64–66). More recently, several studies on
397 human viruses (two herpesviruses and one RNA virus) have shown that the metabolic
398 state of an infected cell can be shifted toward energy generation to support viral
399 replication (65). These studies have highlighted the increasing abundance—up to 48 h
400 after HCV infection—of enzymes involved in *β*-oxidation, amino acid catabolism,

and the TCA cycle (67) and an increase in cellular $\beta$-oxidation following the release of free fatty acids caused by Dengue virus-induced autophagy (68). Among algal viruses, EhV remodels the transcription of host lipid genes for fatty acid synthesis to support viral assembly (69) and also to generate triacylglycerols stored in the virion and available as an energy pool in later infection phases (70). Besides diverting the host metabolism, EhV encodes seven proteins involved in the sphingolipid biosynthesis pathway (71). This pathway produces a viral sphingolipid that is a central component of EhV lipid membranes and that can also act as a signaling lipid and induce programed cell death during the lytic infection phase (72). EhV also encodes a triglyceride lipase (with detectable homology to predicted PkV RF01 lipases ORF 635 and ORF653) that is highly expressed during late infection concomitantly with significant up-regulation of host $\beta$-oxidation genes (69). These examples and our observations of several genes involved in $\beta$-oxidation clearly show that viruses can introduce new metabolism-related genes, sometimes representing entire pathways, into the host, most likely to satisfy the high metabolic requirement of these giant viruses.

## High representation of glycosyltransferases

Compared with other viruses, PkV RF01 was found to encode an unusually high number of glycosyltransferases (GTs) as well as other carbohydrate-active enzymes. Automated annotation of GTs (and other carbohydrate-active enzymes) in reference viral proteomes using dbCAN2 (73) revealed that the largest number of GT domains was encoded by PkV RF01 ($n$ = 48), followed by CeV ($n$ = 13), *Mimivirus* members, and CroV and AaV ($n$ = 8–10) (Fig. 12). We uncovered 48 GT domains encoded in 40 ORFs, 8 of which were predicted to encode more than one GT domain. These domains correspond to 16 different GT families. Most domains were inferred to be

functional, as 31 out of 48 covered at least 70% of the dbCAN2 reference domain, with coverage ranging from 44% to 99%. GTs were found scattered across the genome of PkV RF01 but with some local clustering (Fig. 2A), the latter indicating possible involvement in the same pathway. GT32 was the most represented domain, with 11 proteins (as annotated by dbCAN2) and potentially three additional proteins (ORFs 40, 84, and 861). Eight proteins possessed a GT25 domain that can catalyze the transfer of various sugars onto a growing lipopolysaccharide chain during its biosynthesis. Among these eight predicted ORFs, four contained an additional non-overlapping GT domain (two GT2s, one GT6, and one GT60). Functional analyses of GTs in mimiviruses (or in related *Paramecium bursaria* Chlorella viruses) have demonstrated that some of these enzymes are functional, being able to modify viral collagen-like proteins (74) and polymerize sugars (75). Conservation between PkV RF01 GTs and functionally characterized GTs in viruses and cells is absent or extremely low, which precludes any predictions as to the specific roles of these enzymes in the PkV RF01 life cycle. Nevertheless, this putative glycosylation-conducive autonomy possibly allows the virus to infect a variety of hosts, as the virus can modify its own glycans, which are used for host recognition, independently of the host system (76). In alpha-, flavi-, and herpes-viruses, fusion is mediated by viral glycoproteins (40).

Other carbohydrate-active enzymes in the PkV RF01 genome include seven glycoside hydrolases (GHs), four carbohydrate esterases (CEs), one polysaccharide lyase (PL), one carbohydrate-binding module (CBM), and a putative sugar fermentation stimulation protein A (ORF 1003) possibly involved in maltose metabolism. These numbers are not excessively high compared with other viruses. Other detected ORFs were homologous to enzymes involved in carbohydrate

transport and metabolism, notably a transketolase (ORF 528) involved in the pentose phosphate pathway in all organisms and in the Calvin cycle of photosynthetic organisms. Finally, we detected a 6-phosphofructo-2-kinase/fructose-2,6-biphosphatase 2 (ORF 539) and a mannose-1-phosphate guanylyltransferase/mannose-6-phosphate isomerase (ORF 836) respectively involved in fructose and mannose metabolism.

## Conclusions

The haptophyte virus PkV RF01 has been previously shown to have a longer replication cycle and a broader host range compared with other prymnesioviruses and most other algal viruses. Here, we revealed that PkV RF01 has atypical virion morphology and that infections yield several orders of magnitude fewer infectious particles than other tested prymnesioviruses. In-depth phylogenetic analysis using genes conserved in NCLDVs confirmed that PkV RF01 belongs to *Mimiviridae* but is deeply diverged from existing members, although closer to alga-infecting *Mimiviridae* than heterotroph-infecting ones. Unlike other alga-infecting *Mimiviridae*, however, PkV RF01 has a large genome (1.4 Mb) and contains genes coding for two aminoacyl-tRNA synthetases and the complete BER pathway. All these features are conserved in most heterotroph-infecting *Mimiviridae* and therefore must have been lost in other alga-infecting *Mimiviridae*. This outlier virus features an unprecedentedly high number of genes involved in energy metabolism and glycosylation machinery that may enable its longer replication cycle and broader host range compared with other algal viruses. These genomic and phenotypic features are suggestive of a persistent infection behavior that probably evolved in response to the host growth strategy. Because of nutrient limitations, these persistent systems of slow-

475 growing but ubiquitous hosts with less virulent viruses may represent the most
476 common type of virocells in oceans.

# 477 Materials and Methods

## 478 Culturing and infection

479 All algal host cultures were grown in liquid IMR/2 medium consisting of 70% aged
480 seawater, 30% distilled water (25 PSU), and additional selenite (10 nM final
481 concentration). The cultures were kept at 14°C and partially synchronized using a
482 14:10 h light: dark cycle with irradiance of 100 µmol photons $m^{-2}$ $s^{-2}$ supplied by
483 white fluorescent tubes. Viruses were produced by adding freshly produced viral
484 lysate (ca. 2 x $10^8$ VLP/mL), propagated three time on the host before added to
485 exponentially growing host cultures (ca. 5x$10^5$ cells/mL) in a ratio of 1:10 volume.
486 Infection was followed by flow cytometry (FCM) (77, 78) for 72 h by counting viral
487 particles and host cells, as described in (33). Burst size was calculated as the number
488 of viral particles released from each host cell, estimated from the total number of host
489 cells pre-infection and the total number of VLPs produced during the infection cycle
490 (33).

## 491 Infectious progeny

492 The percentage of viral infectious progeny was determined by comparing the most
493 probable number (MPN; endpoint dilution (78)) and flow cytometric total counts of
494 viral particles produced during infection. The number of infectious particles released
495 in a burst was determined based on the percentage of viral infectivity produced during
496 the infection cycle and the burst size. Infectivity was tested using *Haptolina ericin*a
497 UiO028 as a host, and also compared with two other prymnesioviruses, HeV RF02

and PkV RF02 (33), propagated on He UiO028 and *Prymnesium kappa* RCC3423, respectively.

Briefly, 10× dilution were prepared from fresh viral lysate and added to exponentially growing host cells in 96-well microtiter plates (eight replicates for each dilution). The plates were incubated for 7 days under normal incubation conditions. Cell lysis was measured by monitoring *in situ* fluorescence on a plate reader (PerkinElmer EnSpire™ 2300 Multilabel Reader) at 460/680 nm. Numbers of infectious particles were estimated from the proportion of lysed wells using the MPN_ver4.xls excel spreadsheet from (79).

## Sensitivity to chloroform

The effect of chloroform on infectivity, used to infer the presence of a lipid membrane or lipid molecules in the capsid, was tested by adding 50% (v/v) chloroform to PkV RF01 lysate. After mixing, the chloroform phase was separated from the solution by centrifugation at 4,000 *g* for 5 min. The tubes were incubated at 37°C for 2 h with the lids open to allow evaporation of any remaining chloroform.

Triplicates of exponentially growing He UiO028 cells (1,6 x $10^5$ cells /mL) were incubated with 1:10 volumes of chloroform-treated viruses (ca. 2 x $10^8$ VLP/mL). The incubation was followed for 7 days by counting host cells by FCM (78). Host cells in chloroform-treated or untreated medium at the same ratio used with the viral lysate were used as controls. Virus propagation was confirmed in lysed cultures by FCM.

## Cryo-electron tomography

A small drop of concentrated PkV RF01 (8x109) was deposited on a glow-discharged, 200-mesh copper grid with holey carbon film (R2/1 Cu 200, Quantifoil Micro Tools

GmbH, Germany). The sample was blotted with filter paper and immediately plunge frozen in liquid ethane. Grids were transferred under liquid nitrogen to a cryo-transfer tomography holder (Fishione Instruments, USA) and inserted in a 200-kV transmission electron microscope (Thermo Scientific Talos F200C) equipped with a Ceta 16M camera. Tilt series were recorded at 45,000× magnification and −7 µm defocus between −60° to 60° in 2° increments. Finally, reconstruction, segmentation, and visualization of the tomograms was performed with IMOD v4.9 software (80).

## Purification of viral particles and DNA isolation

Exponentially growing He UiO028 cultures (2 L) were infected with 20 mL of PkV RF01 and inspected visually for lysis. An uninfected culture (100 mL) was used as a control. Lysed algal cultures were checked for viruses by FCM counting. Lysed cultures were first centrifuged to remove algal debris and some bacteria (5,500 rpm for 15 min). Viruses were then pelleted by ultracentrifugation at 25,000 rpm in a Beckman Coulter Optima L90K ultracentrifuge for 2 h. The pellets were resuspended in SM buffer (0.1 M NaCl, 8 mM $MgSO_4 \cdot 7H_20$, 50 mM Tris-HCl, and 0.005% glycerin). Viral particles were further purified by Optiprep gradient centrifugation (81). Fractions were checked for viruses by FCM and for infectivity by infection of He UiO028.

Isolation of high-quality DNA for sequencing was done by following the protocol of (82) with some modifications. Viral particles were disrupted by one round of heating to 90°C for 2 min and then chilling on ice for 2 min. Disodium ethylenediaminetetraacetic acid and proteinase K at a final concentration of 20 mM and 100 µg $mL^{-1}$, respectively, were then added before incubation of the samples for 10 min at 55°C. Sodium dodecyl sulfate at a final concentration of 0.5% (w/v) was subsequently added, and samples were incubated for an additional 1 h at 55°C.

Double-stranded DNA was then purified from the lysates using a Zymo Genomic DNA Clean & Concentrator Kit-10 (Zymo Research, Irvine, CA, USA) according to the manufacturer's protocols. To avoid shearing DNA, gentle pipetting and mixing (accomplished by turning the tubes instead of vortexing) were performed in all steps.

## Genome assembly

Isolated DNA from PkV RF01 was subjected to Illumina TruSeq PCR-free library preparation (insert size 350 bp). The generated library was sequenced on an Illumina MiSeq instrument in paired-end mode (2 × 300 bp) to yield approximately 1.9 million reads, which corresponds to about 400× coverage. Reads were assembled into 2,498 contigs of 500 bp or more with a total assembly size of 4.75 Mb using Newbler (83). In addition, a ligation-based $1D^2$ nanopore library (LSK-308) was constructed and sequenced using an Oxford Nanopore MinION Mk1b device and a FLO-MIN107 flow cell, which resulted in 825 long reads with an N50 of 13.6 kb and a total of 9.89 Mb. To improve the assembly, short-read contigs were manually bridged with the long reads. Manual assembly using Consed (84) yielded a linear genome sequence of 1.4 Mb with inverted terminal repeats. After assembly, the consensus was polished using Nanopolish (85) and Pilon (86).

## Phylogenetic analyses

### Five core genes, SDHA, and SDHB

The phylogenetic position of PkV RF01 was inferred from concatenated protein alignments of five core nucleocytoplasmic virus orthologous genes (NCVOGs) (87): D5-like helicase-primase (NCVOG0023), DNA polymerase elongation subunit family B (NCVOG0038), DNA or RNA helicases of superfamily II (NCVOG0076), packaging ATPase (NCVOG0249), and Poxvirus Late Transcription Factor VLTF3-

like (NCVOG0262). Sequences were obtained from the NCVOG database (ftp.ncbi.nlm.nih.gov/pub/wolf/COGs/NCVOG/) (88). Additional sequences were obtained from genomes retrieved from GenBank and annotated with HMMER v3.12b using the hmmsearch (89) command with hidden Markov models available in Schulz et al. (2017) (13). Sequences from each NCVOG were aligned independently using MAFFT L-INS-i (90). The alignments were trimmed with trimAl v1.2 in *gapyout* mode (91) prior to concatenation using a custom Python script. Bayesian phylogenetic trees were inferred with PhyloBayes 1.7 (92) using the CAT model and a GTR substitution matrix. Four chains were run for 34,500–35,500 generations. The *bpcomp* command was used to check for convergence and stop when *maxdiff* = 0.3. One chain was discarded, and a consensus tree was constructed using the remaining three chains.

For phylogenetic analyses of succinate dehydrogenase subunits, top hits of PkV RF01 SDHA and SDHB were retrieved from UniProt (https://www.uniprot.org/) using online PHMMR searches (https://www.ebi.ac.uk/Tools/hmmer/search/phmmer) and also from the *Tara* Oceans project using online BLASTP searches (http://tara-oceans.mio.osupytheas.fr/ocean-gene-atlas/) (Villar et al., 2018). Alignments generated with MAFFT L-INS-i were filtered with trimAl in gapyout mode. Maximum-likelihood phylogenies were inferred with RAxML 8.2.9 (93) using the PROTCATALG model and automatic bootstrapping with the following options: '-N autoMRE -f a -n autoresult'. Phylogenetic trees of PkV RF01, SDHA, and SDHB were visualized using iTOL (94).

### Rpb2, IleRS, and AsnRS

To reconstruct a phylogenetic tree based on the second largest RNA polymerase subunit, homologs were recruited by comparing Mimivirus Rpb2 against all proteins

of viruses and selected organisms in the KEGG database using the GenomeNet BLASTP tool (https://www.genome.jp/). Organisms were manually selected from the KEGG list to ensure broad taxonomic coverage of the tree of life. The retrieved amino acid sequences were aligned using MAFFT-LINSI (90) and then trimmed using trimAl (91) with the following parameters: '-resoverlap 0.5 -seqoverlap 70 -gt 0.8 -st 0.001 -cons 50'. The tree was reconstructed using FastTree (95) as implemented in the GenomeNet TREE tool (https://www.genome.jp/tools-bin/ete). Isoleucine tRNA synthase and aspartyl tRNA synthetase viral and cellular homologs were retrieved and aligned in the same way. Trees were searched using PhyloBayes MPI (96) with the non-homogeneous CAT+GTR model (97). For each protein three chains were run until *maxdiff* parameter reach < 0.3 (0.27 for AsnRS and 0.16 for IleRS). One chain was discarded for IleRS, and a consensus tree was constructed using the remaining chains.

## Gene prediction and functional and taxonomic annotation

GeneMarkS with the option 'virus' (98) predicted 1,121 open reading frames (ORFs) in the fully assembled genome sequence of PkV RF01, while tRNAscan-SE (99) predicted 41 tRNAs. PkV RF01 CDS amino acid sequences were searched against Virus-Host DB (100), RefSeq (101), UniRef90 (102), and COG (61) databases using BLASTP with an *E*-value of $1 \times 10^{-5}$ as the significant similarity threshold and against the Conserved Domain Database (103) using RPS-BLAST with an *E*-value threshold of $1 \times 10^{-2}$. The 10 best hits for each database were compiled in a single file and manually inspected to transfer annotations of subject sequences to our query. In ambiguous cases, such as distant homologs (often seen in viral genomes) or unclear or contradictory annotations of subject sequences, the query was searched against KEGG genes (104) to allow extensive manual checking using GenomeNet tools

(https://www.genome.jp/; alignment quality, length comparison to canonical genes, and links with KEGG orthology). We automatically annotated glycosyltransferases (GTs) and other carbohydrate-active enzymes (glycoside hydrolases, GHs; polysaccharide lyases, PLs; carbohydrate esterases, CEs; and auxiliary activities, AAs) in PkV RF01 and all viral genomes in Virus-Host DB (as of June 2018) using the *hmm* option of the dbCAN2 pipeline and its profile database (73). We retained hits with *E*-values < $1 \times 10^{-5}$ and domain coverage > 35%, which corresponded to default settings.

## Taxonomic and functional analysis of vSDHA homologs in OM-RGCv1

We searched PkV RF01 SDHA and SDHB against OM-RGCv1 (105) using the Ocean Gene Atlas (106) BLAST-based tool and kept the top 50 hits with significant *E*-values for further analysis. We then collected genome fragments (contigs) encoding these 50 SDHAs and 50 SDHBs by searching via BLASTN for identical hits over full *SDHA* or *SDHB* lengths against *Tara* ocean assemblies (downloaded from EBI) used to construct OM-RGCv1. We predicted ORFs in these genome fragments using GeneMarkS. The resulting 1,113 amino acid sequences were functionally annotated by searching against Pfam protein families (107) using profile HMM scan (108) and also taxonomically using a last common ancestor strategy as in (109); in brief, protein sequences were searched against a database composed of UniRef cells, MMETSP (110) and Virus-Host DB (100) data using DIAMOND (111). Selected hits were then used to derive the last common ancestor of the query using a NCBI taxonomic tree re-wired to reflect the taxonomy of NCLDVs.

## PCR and RT-PCR optimization

We designed specific primers (Table 3) targeting a 256-bp region of the *mcp* gene to use both as an internal control in the RT-PCR and to confirm that our protocols were optimized. For each PCR, a negative control (sterile distilled $H_2O$) was included. PCR amplifications were carried out in 50-µL total volumes containing 1 µL of template using a DNA HotStarTaq Master Mix kit (Qiagen). The cycling protocol was as follows: 15 min at 95°C, followed by 35 cycles of 30 s at 94°C, 30 s at 59°C, and 30 s at 72°C, with a final extension of 12 min at 72°C.

RT-PCRs were performed using the SuperScript III One-Step RT-PCR with Platinum *Taq* DNA Polymerase system (Thermo Fisher). Cycling conditions were as follows: 16 min at 55°C and 2 min at 94°C, followed by 40 cycles of 15 s at 94°C, 30 s at 49°C, and 30 s at 68°C, and a final extension of 5 min at 68°C.

All PCR products were checked for the correct size on a 1.5% agarose gel stained with GelRed (Biotium). PCR products were further checked by sequencing using BigDye v3.1 (Thermo Fisher) for cycle sequencing (Sekvenseringslaboratoriet, UiB, Norway).

## PCR amplification and RT-PCR analysis of *vSDHA*

To investigate whether the *vSDHA* gene is transcribed during infection, an infected culture of He_UiO028 plus PkV RF01 as well as an uninfected He UiO028 culture (control) were set up as described above. Samples were collected at 24, 72, and 96 h post infection from both cultures. RNA was extracted using an RNeasy Plus Universal Mini kit (Qiagen), with gDNA removed in an extra step using a TURBO DNA-free kit (Ambion).

Specific primers were designed to target a 150-bp region of the *vSDHA* gene (Table 3). For each PCR, two negative controls (sterile distilled $H_2O$ and extracted DNA from He028) were included. As positive controls for the transcription, we used primers targeting the *mcp* gene (see above). As a positive PCR control, we used genomic PkV RF01 DNA. PCR amplifications were conducted in 50-µL total volumes containing 1 µL of template DNA using an ExTaq kit (Takara). The cycling protocol was as follows: 5 min at 94°C, followed by 35 cycles of 30 s at 94°C, 30 s at 59°C, and 30 s at 72°C, with a final extension of 12 min extension at 72°C.

RT-PCRs were performed using a SuperScript III One-Step RT-PCR with Platinum Taq DNA Polymerase system (Thermo Fisher). Cycling conditions were as follows: 16 min at 55°C and 2 min at 94°C, followed by 40 cycles of 15 s at 94°C, 30 s at 49°C, and 30 s at 68°C, with a final extension of 5 min at 68°C. PCR products were checked as described above.

## Data availability

Raw sequence reads and PkV RF01 genome sequence were deposited at the European Bioinformatics Institute (EMBL-EBI) (https://www.ebi.ac.uk) under project name PRJEB37450. The complete video records of a cryo-electron tomogram of a PkV RF01 virion and sequence data as well as curated gene annotation table as reported in this study are available at https://github.com/RomainBlancMathieu/PkV-RF01.

## Acknowledgements

The recording of tilt series was performed with the help of Sebastian Schultz at the Unit of Cellular Electron Microscopy, the Norwegian Radium Hospital. Initial sequencing (MiSeq and Pacbio) of PkV RF01 total DNA was performed at the Norwegian Sequencing Center (https://www.sequencing.uio.no/). We thank Hilde M. K. Stabell and Solveig Siqveland, Department of Biological Sciences, University of Bergen, Norway, for technical assistance with molecular biology experiments as well as Christian Rückert, Bielefeld University, for support in manual finishing of genome assembly and Minyue Fan, Kyoto University, for assistance in genes analysis. This

work was supported by the Research Council of Norway project entitled "Uncovering the key players for regulation of phytoplankton function and structure: lesson to be learned from algal virus-haptophyte coexistence" (VirVar, project number 294364 to RAS). Additional funding was provided by the European Union Horizons 2020 research and innovation program, grant agreement no. 685778 ("Virus-X") to RAS and DB. This work was also supported by the Future Development Funding Program of the Kyoto University Research Coordination Alliance. HO was supported by JSPS/KAKENHI (No. 18H02279), and Scientific Research on Innovative Areas from the Ministry of Education, Culture, Science, Sports and Technology (MEXT) of Japan (Nos. 16H06429, 16K21723, 16H06437). The Super Computer System, Institute for Chemical Research, Kyoto University, provided computational time. We thank Barbara Goodson, from Edanz Group (www.edanzediting.com/ac), for editing the English text of a draft of this manuscript.

## Competing interests

Authors declare having no competing interests.

## References

1. Dupré JO. 2009. Varieties of Living Things: Life at the Intersection of Lineage and Metabolism. Philosophy & Theory in Biology 1.

2. Forterre P. 2012. Virocell Concept, The, p. a0023264. *In* John Wiley & Sons, Ltd (ed.), eLS. John Wiley & Sons, Ltd, Chichester, UK.

3. Raoult D, Forterre P. 2008. Redefining viruses: lessons from Mimivirus. Nat Rev Microbiol 6:315–319.

4. Claverie J-M. 2006. Viruses take center stage in cellular evolution. Genome Biology 7:110.

5. Mann NH, Cook A, Millard A, Bailey S, Clokie M. 2003. Bacterial photosynthesis genes in a virus. Nature 424:741–741.

6. Lindell D, Sullivan MB, Johnson ZI, Tolonen AC, Rohwer F, Chisholm SW. 2004. Transfer of photosynthesis genes to and from Prochlorococcus viruses. PNAS 101:11013–11018.

7. Hurwitz BL, Hallam SJ, Sullivan MB. 2013. Metabolic reprogramming by viruses in the sunlit and dark ocean. Genome Biol 14:R123.

8. Thompson LR, Zeng Q, Kelly L, Huang KH, Singer AU, Stubbe J, Chisholm SW. 2011. Phage auxiliary metabolic genes and the redirection of cyanobacterial host carbon metabolism. Proc Natl Acad Sci USA 108:E757-764.

9. Anantharaman K, Duhaime MB, Breier JA, Wendt KA, Toner BM, Dick GJ. 2014. Sulfur Oxidation Genes in Diverse Deep-Sea Viruses. Science 344:757–760.

10. Lindell D, Jaffe JD, Johnson ZI, Church GM, Chisholm SW. 2005. Photosynthesis genes in marine viruses yield proteins during host infection. Nature 438:86–89.

11. Fridman S, Flores-Uribe J, Larom S, Alalouf O, Liran O, Yacoby I, Salama F, Bailleul B, Rappaport F, Ziv T, Sharon I, Cornejo-Castillo FM, Philosof A, Dupont CL, Sánchez P, Acinas SG, Rohwer FL, Lindell D, Béjà O. 2017. A myovirus encoding both photosystem I and II proteins enhances cyclic electron flow in infected Prochlorococcus cells. Nat Microbiol 2:1350–1357.

12. Raoult D, Audic S, Robert C, Abergel C, Renesto P, Ogata H, La Scola B, Suzan M, Claverie J-M. 2004. The 1.2-megabase genome sequence of Mimivirus. Science 306:1344–1350.

13. Schulz F, Yutin N, Ivanova NN, Ortega DR, Lee TK, Vierheilig J, Daims H, Horn M, Wagner M, Jensen GJ, Kyrpides NC, Koonin EV, Woyke T. 2017. Giant viruses with an expanded complement of translation system components. Science 356:82–85.

14. Abrahão J, Silva L, Silva LS, Khalil JYB, Rodrigues R, Arantes T, Assis F, Boratto P, Andrade M, Kroon EG, Ribeiro B, Bergier I, Seligmann H, Ghigo E, Colson P, Levasseur A, Kroemer G, Raoult D, Scola BL. 2018. Tailed giant Tupanvirus possesses the most complete translational apparatus of the known virosphere. Nat Commun 9:1–12.

15. Miller ES, Heidelberg JF, Eisen JA, Nelson WC, Durkin AS, Ciecko A, Feldblyum TV, White O, Paulsen IT, Nierman WC, Lee J, Szczypinski B, Fraser CM. 2003. Complete Genome Sequence of the Broad-Host-Range Vibriophage KVP40: Comparative Genomics of a T4-Related Bacteriophage. J Bacteriol 185:5220–5233.

16. Yoshikawa G, Askora A, Blanc-Mathieu R, Kawasaki T, Li Y, Nakano M, Ogata H, Yamada T. 2018. Xanthomonas citri jumbo phage XacN1 exhibits a wide host range and high complement of tRNA genes. Sci Rep 8:4486.

17. Mizuno CM, Guyomar C, Roux S, Lavigne R, Rodriguez-Valera F, Sullivan MB, Gillet R, Forterre P, Krupovic M. 2019. Numerous cultivated and uncultivated viruses encode ribosomal proteins. Nature Communications 10:752.

18. Schvarcz CR, Steward GF. 2018. A giant virus infecting green algae encodes key fermentation genes. Virology 518:423–433.

19. Piacente F, Gaglianone M, Laugieri ME, Tonetti MG. 2015. The Autonomous Glycosylation of Large DNA Viruses. International Journal of Molecular Sciences 16:29315–29328.

20. Schulz F, Roux S, Paez-Espino D, Jungbluth S, Walsh D, Denef VJ, McMahon KD, Konstantinidis KT, Eloe-Fadrosh EA, Kyrpides N, Woyke T. 2020. Giant virus diversity and host interactions through global metagenomics. Nature 1–7.

21. Needham DM, Yoshizawa S, Hosaka T, Poirier C, Choi CJ, Hehenberger E, Irwin NAT, Wilken S, Yung C-M, Bachy C, Kurihara R, Nakajima Y, Kojima K, Kimura-Someya T, Leonard G, Malmstrom RR, Mende DR, Olson DK, Sudo Y, Sudek S, Richards TA, DeLong EF, Keeling PJ, Santoro AE, Shirouzu M, Iwasaki W, Worden AZ. 2019. A distinct lineage of giant viruses brings a rhodopsin photosystem to unicellular marine predators. PNAS 116:20574–20583.

22. Roux S, Brum JR, Dutilh BE, Sunagawa S, Duhaime MB, Loy A, Poulos BT, Solonenko N, Lara E, Poulain J, Pesant S, Kandels-Lewis S, Dimier C, Picheral M, Searson S, Cruaud C, Alberti A, Duarte CM, Gasol JM, Vaqué D, Bork P, Acinas SG, Wincker P, Sullivan MB. 2016. Ecogenomics and potential biogeochemical impacts of globally abundant ocean viruses. Nature 537:689–693.

23. Nishimura Y, Watai H, Honda T, Mihara T, Omae K, Roux S, Blanc-Mathieu R, Yamamoto K, Hingamp P, Sako Y, Sullivan MB, Goto S, Ogata H, Yoshida T. 2017. Environmental Viral Genomes Shed New Light on Virus-Host Interactions in the Ocean. mSphere 2.

24. Forterre P. 2013. The virocell concept and environmental microbiology. ISME J 7:233–236.

25. Rosenwasser S, Ziv C, Creveld SG van, Vardi A. 2016. Virocell Metabolism: Metabolic Innovations During Host–Virus Interactions in the Ocean. Trends in Microbiology 24:821–832.

26. Coy SR, Gann ER, Pound HL, Short SM, Wilhelm SW. 2018. Viruses of Eukaryotic Algae: Diversity, Methods for Detection, and Future Directions. Viruses 10:487.

27. Gallot-Lavallée L, Blanc G, Claverie J-M. 2017. Comparative Genomics of Chrysochromulina Ericina Virus and Other Microalga-Infecting Large DNA Viruses Highlights Their Intricate Evolutionary Relationship with the Established Mimiviridae Family. Journal of Virology 91:e00230-17.

28. Jacobsen A, Bratbak G, Heldal M. 1996. Isolation and characterization of a virus infecting phaeocystis pouchetii (prymnesiophyceae)1. Journal of Phycology 32:923–927.

29. Baudoux A-C, Brussaard CPD. 2005. Characterization of different viruses infecting the marine harmful algal bloom species Phaeocystis globosa. Virology 341:80–90.

30. Wagstaff BA, Vladu IC, Barclay JE, Schroeder DC, Malin G, Field RA. 2017. Isolation and Characterization of a Double Stranded DNA Megavirus Infecting the Toxin-Producing Haptophyte Prymnesium parvum. Viruses 9.

812 31. Egge ES, Johannessen TV, Andersen T, Eikrem W, Bittner L, Larsen A, Sandaa
813 R-A, Edvardsen B. 2015. Seasonal diversity and dynamics of haptophytes in the
814 Skagerrak, Norway, explored by high-throughput sequencing. Mol Ecol
815 24:3026–3042.

816 32. Sandaa RA, Heldal M, Castberg T, Thyrhaug R, Bratbak G. 2001. Isolation and
817 characterization of two viruses with large genome size infecting
818 Chrysochromulina ericina (Prymnesiophyceae) and Pyramimonas orientalis
819 (Prasinophyceae). Virology 290:272–280.

820 33. Johannessen TV, Bratbak G, Larsen A, Ogata H, Egge ES, Edvardsen B, Eikrem
821 W, Sandaa R-A. 2015. Characterisation of three novel giant viruses reveals huge
822 diversity among viruses infecting Prymnesiales (Haptophyta). Virology
823 476:180–188.

824 34. Feldman HA, Wang SS. 1961. Sensitivity of Various Viruses to Chloroform.
825 Proceedings of the Society for Experimental Biology and Medicine 106:736–
826 738.

827 35. Martínez M, Boere A, Gilg I, van Lent J, Witte H, van Bleijswijk J, Brussaard C.
828 2015. New lipid envelope-containing dsDNA virus isolates infecting
829 Micromonas pusilla reveal a separate phylogenetic group. Aquatic Microbial
830 Ecology 74:17–28.

831 36. Mirza SF, Staniewski MA, Short CM, Long AM, Chaban YV, Short SM. 2015.
832 Isolation and characterization of a virus infecting the freshwater algae
833 Chrysochromulina parva. Virology 486:105–115.

834 37. Mackinder LCM, Worthy CA, Biggi G, Hall M, Ryan KP, Varsani A, Harper
835 GM, Wilson WH, Brownlee C, Schroeder DC. 2009. A unicellular algal virus,
836 Emiliania huxleyi virus 86, exploits an animal-like infection strategy. Journal of
837 General Virology, 90:2306–2316.

838 38. Huiskonen JT, Kivelä HM, Bamford DH, Butcher SJ. 2004. The PM2 virion has
839 a novel organization with an internal membrane and pentameric receptor binding
840 spikes. Nat Struct Mol Biol 11:850–856.

841 39. Yan X, Chipman PR, Castberg T, Bratbak G, Baker TS. 2005. The Marine Algal
842 Virus PpV01 Has an Icosahedral Capsid with T=219 Quasisymmetry. J Virol
843 79:9236–9243.

844 40. Huiskonen JT, Butcher SJ. 2007. Membrane-containing viruses with
845 icosahedrally symmetric capsids. Curr Opin Struct Biol 17:229–236.

846 41. King AM, Lefkowitz E, Adams MJ, Carstens EB. 2011. Virus Taxonomy: Ninth
847 Report of the International Committee on Taxonomy of Viruses. Elsevier.

848 42. Peralta B, Gil-Carton D, Castaño-Díez D, Bertin A, Boulogne C, Oksanen HM,
849 Bamford DH, Abrescia NGA. 2013. Mechanism of Membranous Tunnelling
850 Nanotube Formation in Viral Genome Delivery. PLOS Biology 11:e1001667.

851 43. Philippe C, Krupovic M, Jaomanjaka F, Claisse O, Petrel M, le Marrec C. 2018.
852 Bacteriophage GC1, a Novel Tectivirus Infecting Gluconobacter Cerinus, an
853 Acetic Acid Bacterium Associated with Wine-Making. Viruses 10.

854 44. Yan X, Yu Z, Zhang P, Battisti AJ, Chipman PR, Bajaj C, Bergoin M,
855 Rossmann MG, Baker TS. 2009. The Capsid Proteins of a Large, Icosahedral
856 dsDNA Virus. J Mol Biol 385:1287–1299.

857 45. Klose T, Rossmann MG. 2014. Structure of large dsDNA viruses. Biol Chem
858 395:711–719.

859 46. Gowing MM. 1993. Large virus-like particles from vacuoles of phaeodarian
860 radiolarians and from other marine samples. Marine Ecology Progress Series
861 101:33–43.

862 47. Gromov BV, Mamkaeva KA. 1981. A virus infection in the synchronized
863 population of the *Chlorococcum minutum* zoospores. Algological Studies/Archiv
864 für Hydrobiologie, Supplement Volumes 252–259.

865 48. Bratbak G, Jacobsen A, Heldal M, Nagasaki K, Thingstad F. 1998. Virus
866 production in Phaeocystis pouchetii and its relation to host cell growth and
867 nutrition. Aquatic Microbial Ecology 16:1–9.

868 49. Zimmerman AE, Bachy C, Ma X, Roux S, Jang HB, Sullivan MB, Waldbauer
869 JR, Worden AZ. 2019. Closely related viruses of the marine picoeukaryotic alga
870 Ostreococcus lucimarinus exhibit different ecological strategies. Environ
871 Microbiol 21:2148–2170.

872 50. Thomsen HA, Buck KR, Chavez FP. 1994. Haptophytes as components of
873 marine phytoplankton. DTU Research Database 187–208.

874 51. Berngruber TW, Froissart R, Choisy M, Gandon S. 2013. Evolution of Virulence
875 in Emerging Epidemics. PLOS Pathogens 9:e1003209.

876 52. Day T, Proulx SR. 2004. A General Theory for the Evolutionary Dynamics of
877 Virulence. The American Naturalist 163:E40–E63.

878 53. King AA, Shrestha S, Harvill ET, Bjørnstad ON. 2009. Evolution of Acute
879 Infections and the Invasion-Persistence Trade-Off. The American Naturalist
880 173:446–455.

881 54. Brussaard CPD, Bratbak G, Baudoux A-C, Ruardij P. 2007. Phaeocystis and its
882 interaction with viruses. Biogeochemistry 83:201–215.

883 55. Leggett HC, Buckling A, Long GH, Boots M. 2013. Generalism and the
884 evolution of parasite virulence. Trends Ecol Evol (Amst) 28:592–596.

885 56. Woolhouse MEJ, Taylor LH, Haydon DT. 2001. Population Biology of
886 Multihost Pathogens. Science 292:1109–1112.

887 57. Johannessen TV, Larsen A, Bratbak G, Pagarete A, Edvardsen B, Egge ED,
888 Sandaa R-A. 2017. Seasonal Dynamics of Haptophytes and dsDNA Algal
889 Viruses Suggest Complex Virus-Host Relationship. Viruses 9.

890 58. Gran-Stadniczeñko S, Krabberød AK, Sandaa R-A, Yau S, Egge E, Edvardsen
891 B. 2019. Seasonal Dynamics of Algae-Infecting Viruses and Their Inferred
892 Interactions with Protists. Viruses 11:1043.

893 59. Fischer MG, Allen MJ, Wilson WH, Suttle CA. 2010. Giant virus with a
894 remarkable complement of genes infects marine zooplankton. Proc Natl Acad
895 Sci USA 107:19508–19513.

896 60. Sandaa R-A, Dahle H, Brussaard CPD, Ogata H, Blanc-Mathieu R. Algal
897 viruses belonging to a subgroup within the Mimiviridae familyEncyclopedia of
898 Virology, 4th ed. Bamford, D., M. Zuckerman, Elsevier, Academic.

899 61. Tatusov RL, Galperin MY, Natale DA, Koonin EV. 2000. The COG database: a
900 tool for genome-scale analysis of protein functions and evolution. Nucleic Acids
901 Res 28:33–36.

902 62. Blanc-Mathieu R, Ogata H. 2016. DNA repair genes in the Megavirales
903 pangenome. Current Opinion in Microbiology 31:94–100.

904 63. Moniruzzaman M, Martinez-Gutierrez CA, Weinheimer AR, Aylward FO. 2020.
905 Dynamic genome evolution and complex virocell metabolism of globally-
906 distributed giant viruses. 1. Nature Communications 11:1710.

907 64. Ono A. 2010. Viruses and Lipids. Viruses 2:1236–1238.

908 65. Heaton NS, Randall G. 2011. Multifaceted roles for lipids in viral infection.
909 Trends Microbiol 19:368–375.

910 66. Lange PT, Lagunoff M, Tarakanova VL. 2019. Chewing the Fat: The Conserved
911 Ability of DNA Viruses to Hijack Cellular Lipid Metabolism. Viruses 11:119.

912 67. Diamond DL, Syder AJ, Jacobs JM, Sorensen CM, Walters K-A, Proll SC,
913 McDermott JE, Gritsenko MA, Zhang Q, Zhao R, Metz TO, Camp DG, Waters
914 KM, Smith RD, Rice CM, Katze MG. 2010. Temporal Proteome and Lipidome
915 Profiles Reveal Hepatitis C Virus-Associated Reprogramming of Hepatocellular
916 Metabolism and Bioenergetics. PLoS Pathog 6.

917 68. Heaton NS, Randall G. 2010. Dengue virus induced autophagy regulates lipid
918 metabolism. Cell Host Microbe 8:422–432.

919 69. Rosenwasser S, Mausz MA, Schatz D, Sheyn U, Malitsky S, Aharoni A,
920 Weinstock E, Tzfadia O, Ben-Dor S, Feldmesser E, Pohnert G, Vardi A. 2014.
921 Rewiring Host Lipid Metabolism by Large Viruses Determines the Fate of
922 Emiliania huxleyi, a Bloom-Forming Alga in the Ocean[C][W][OPEN]. Plant
923 Cell 26:2689–2707.

924 70. Malitsky S, Ziv C, Rosenwasser S, Zheng S, Schatz D, Porat Z, Ben-Dor S,
925 Aharoni A, Vardi A. 2016. Viral infection of the marine alga Emiliania huxleyi

triggers lipidome remodeling and induces the production of highly saturated triacylglycerol. New Phytologist 210:88–96.

71. Wilson WH, Schroeder DC, Allen MJ, Holden MTG, Parkhill J, Barrell BG, Churcher C, Hamlin N, Mungall K, Norbertczak H, Quail MA, Price C, Rabbinowitsch E, Walker D, Craigon M, Roy D, Ghazal P. 2005. Complete Genome Sequence and Lytic Phase Transcription Profile of a Coccolithovirus. Science 309:1090–1092.

72. Vardi A, Van Mooy BAS, Fredricks HF, Popendorf KJ, Ossolinski JE, Haramaty L, Bidle KD. 2009. Viral glycosphingolipids induce lytic infection and cell death in marine phytoplankton. Science 326:861–865.

73. Zhang H, Yohe T, Huang L, Entwistle S, Wu P, Yang Z, Busk PK, Xu Y, Yin Y. 2018. dbCAN2: a meta server for automated carbohydrate-active enzyme annotation. Nucleic Acids Res 46:W95–W101.

74. Luther KB, Hülsmeier AJ, Schegg B, Deuber SA, Raoult D, Hennet T. 2011. Mimivirus collagen is modified by bifunctional lysyl hydroxylase and glycosyltransferase enzyme. J Biol Chem 286:43701–43709.

75. Rommel AJ, Hülsmeier AJ, Jurt S, Hennet T. 2016. Giant mimivirus R707 encodes a glycogenin paralogue polymerizing glucose through α- and β-glycosidic linkages. Biochem J 473:3451–3462.

76. Parakkottil Chothi M, Duncan GA, Armirotti A, Abergel C, Gurnon JR, Van Etten JL, Bernardi C, Damonte G, Tonetti M. 2010. Identification of an l-Rhamnose Synthetic Pathway in Two Nucleocytoplasmic Large DNA Viruses. J Virol 84:8829–8838.

77. Marie D, Brussaard CPD, Thyrhaug R, Bratbak G, Vaulot D. 1999. Enumeration of Marine Viruses in Culture and Natural Samples by Flow Cytometry. Appl Environ Microbiol 65:45–52.

78. Brussaard CPD. 2004. Optimization of procedures for counting viruses by flow cytometry. Appl Environ Microbiol 70:1506–1513.

79. Jarvis B, Wilrich C, Wilrich P-T. 2010. Reconsideration of the derivation of Most Probable Numbers, their standard deviations, confidence bounds and rarity values. J Appl Microbiol 109:1660–1667.

80. Kremer JR, Mastronarde DN, McIntosh JR. 1996. Computer visualization of three-dimensional image data using IMOD. J Struct Biol 116:71–76.

81. Lawrence JE, Steward GF. 2010. Purification of viruses by centrifugation, p. 166–181. *In* Wilhelm, S, Weinbauer, M, Suttle, C (eds.), Manual of Aquatic Viral Ecology. American Society of Limnology and Oceanography.

82. Sandaa R-A, E. Storesund J, Olesin E, Lund Paulsen M, Larsen A, Bratbak G, Ray JL. 2018. Seasonality Drives Microbial Community Structure, Shaping both Eukaryotic and Prokaryotic Host–Viral Relationships in an Arctic Marine Ecosystem. Viruses 10.

966 83. Margulies M, Egholm M, Altman WE, Attiya S, Bader JS, Bemben LA, Berka J,
967 Braverman MS, Chen Y-J, Chen Z, Dewell SB, Du L, Fierro JM, Gomes XV,
968 Godwin BC, He W, Helgesen S, Ho CH, Irzyk GP, Jando SC, Alenquer MLI,
969 Jarvie TP, Jirage KB, Kim J-B, Knight JR, Lanza JR, Leamon JH, Lefkowitz
970 SM, Lei M, Li J, Lohman KL, Lu H, Makhijani VB, McDade KE, McKenna
971 MP, Myers EW, Nickerson E, Nobile JR, Plant R, Puc BP, Ronan MT, Roth GT,
972 Sarkis GJ, Simons JF, Simpson JW, Srinivasan M, Tartaro KR, Tomasz A, Vogt
973 KA, Volkmer GA, Wang SH, Wang Y, Weiner MP, Yu P, Begley RF, Rothberg
974 JM. 2005. Genome sequencing in microfabricated high-density picolitre
975 reactors. Nature 437:376–380.

976 84. Gordon D, Green P. 2013. Consed: a graphical editor for next-generation
977 sequencing. Bioinformatics 29:2936–2937.

978 85. Loman NJ, Quick J, Simpson JT. 2015. A complete bacterial genome assembled
979 de novo using only nanopore sequencing data. Nat Methods 12:733–735.

980 86. Walker BJ, Abeel T, Shea T, Priest M, Abouelliel A, Sakthikumar S, Cuomo
981 CA, Zeng Q, Wortman J, Young SK, Earl AM. 2014. Pilon: An Integrated Tool
982 for Comprehensive Microbial Variant Detection and Genome Assembly
983 Improvement. PLOS ONE 9:e112963.

984 87. Yutin N, Wolf YI, Raoult D, Koonin EV. 2009. Eukaryotic large nucleo-
985 cytoplasmic DNA viruses: Clusters of orthologous genes and reconstruction of
986 viral genome evolution. Virology Journal 6:223.

987 88. Yutin N, Wolf YI, Koonin EV. 2014. Origin of giant viruses from smaller DNA
988 viruses not from a fourth domain of cellular life. Virology 466–467:38–52.

989 89. Eddy SR. 2011. Accelerated Profile HMM Searches. PLOS Computational
990 Biology 7:e1002195.

991 90. Katoh K, Standley DM. 2013. MAFFT multiple sequence alignment software
992 version 7: improvements in performance and usability. Mol Biol Evol 30:772–
993 780.

994 91. Capella-Gutiérrez S, Silla-Martínez JM, Gabaldón T. 2009. trimAl: a tool for
995 automated alignment trimming in large-scale phylogenetic analyses.
996 Bioinformatics 25:1972–1973.

997 92. Lartillot N, Lepage T, Blanquart S. 2009. PhyloBayes 3: a Bayesian software
998 package for phylogenetic reconstruction and molecular dating. Bioinformatics
999 25:2286–2288.

1000 93. Stamatakis A. 2014. RAxML version 8: a tool for phylogenetic analysis and
1001 post-analysis of large phylogenies. Bioinformatics 30:1312–1313.

1002 94. Letunic I, Bork P. 2016. Interactive tree of life (iTOL) v3: an online tool for the
1003 display and annotation of phylogenetic and other trees. Nucleic Acids Res
1004 44:W242–W245.

95. Price MN, Dehal PS, Arkin AP. 2009. FastTree: Computing Large Minimum Evolution Trees with Profiles instead of a Distance Matrix. Mol Biol Evol 26:1641–1650.

96. Lartillot N, Rodrigue N, Stubbs D, Richer J. 2013. PhyloBayes MPI: phylogenetic reconstruction with infinite mixtures of profiles in a parallel environment. Syst Biol 62:611–615.

97. Lartillot N, Philippe H. 2004. A Bayesian Mixture Model for Across-Site Heterogeneities in the Amino-Acid Replacement Process. Mol Biol Evol 21:1095–1109.

98. Besemer J, Lomsadze A, Borodovsky M. 2001. GeneMarkS: a self-training method for prediction of gene starts in microbial genomes. Implications for finding sequence motifs in regulatory regions. Nucleic Acids Res 29:2607–2618.

99. Lowe TM, Chan PP. 2016. tRNAscan-SE On-line: integrating search and context for analysis of transfer RNA genes. Nucleic Acids Res 44:W54-57.

100. Mihara T, Nishimura Y, Shimizu Y, Nishiyama H, Yoshikawa G, Uehara H, Hingamp P, Goto S, Ogata H. 2016. Linking Virus Genomes with Host Taxonomy. Viruses 8:66.

101. Pruitt KD, Tatusova T, Maglott DR. 2007. NCBI reference sequences (RefSeq): a curated non-redundant sequence database of genomes, transcripts and proteins. Nucleic Acids Res 35:D61–D65.

102. Suzek BE, Wang Y, Huang H, McGarvey PB, Wu CH. 2015. UniRef clusters: a comprehensive and scalable alternative for improving sequence similarity searches. Bioinformatics 31:926–932.

103. Marchler-Bauer A, Derbyshire MK, Gonzales NR, Lu S, Chitsaz F, Geer LY, Geer RC, He J, Gwadz M, Hurwitz DI, Lanczycki CJ, Lu F, Marchler GH, Song JS, Thanki N, Wang Z, Yamashita RA, Zhang D, Zheng C, Bryant SH. 2015. CDD: NCBI's conserved domain database. Nucleic Acids Res 43:D222–D226.

104. Kanehisa M, Sato Y, Kawashima M, Furumichi M, Tanabe M. 2016. KEGG as a reference resource for gene and protein annotation. Nucleic Acids Res 44:D457–D462.

105. Sunagawa S, Coelho LP, Chaffron S, Kultima JR, Labadie K, Salazar G, Djahanschiri B, Zeller G, Mende DR, Alberti A, Cornejo-Castillo FM, Costea PI, Cruaud C, d'Ovidio F, Engelen S, Ferrera I, Gasol JM, Guidi L, Hildebrand F, Kokoszka F, Lepoivre C, Lima-Mendez G, Poulain J, Poulos BT, Royo-Llonch M, Sarmento H, Vieira-Silva S, Dimier C, Picheral M, Searson S, Kandels-Lewis S, Tara Oceans coordinators, Bowler C, de Vargas C, Gorsky G, Grimsley N, Hingamp P, Iudicone D, Jaillon O, Not F, Ogata H, Pesant S, Speich S, Stemmann L, Sullivan MB, Weissenbach J, Wincker P, Karsenti E, Raes J, Acinas SG, Bork P. 2015. Ocean plankton. Structure and function of the global ocean microbiome. Science 348:1261359.

106. Villar E, Vannier T, Vernette C, Lescot M, Cuenca M, Alexandre A, Bachelerie P, Rosnet T, Pelletier E, Sunagawa S, Hingamp P. 2018. The Ocean Gene Atlas: exploring the biogeography of plankton genes online. Nucleic Acids Res 46:W289–W295.

107. El-Gebali S, Mistry J, Bateman A, Eddy SR, Luciani A, Potter SC, Qureshi M, Richardson LJ, Salazar GA, Smart A, Sonnhammer ELL, Hirsh L, Paladin L, Piovesan D, Tosatto SCE, Finn RD. 2019. The Pfam protein families database in 2019. Nucleic Acids Res 47:D427–D432.

108. Eddy SR. 1998. Profile hidden Markov models. Bioinformatics 14:755–763.

109. Carradec Q, Pelletier E, Silva CD, Alberti A, Seeleuthner Y, Blanc-Mathieu R, Lima-Mendez G, Rocha F, Tirichine L, Labadie K, Kirilovsky A, Bertrand A, Engelen S, Madoui M-A, Méheust R, Poulain J, Romac S, Richter DJ, Yoshikawa G, Dimier C, Kandels-Lewis S, Picheral M, Searson S, Jaillon O, Aury J-M, Karsenti E, Sullivan MB, Sunagawa S, Bork P, Not F, Hingamp P, Raes J, Guidi L, Ogata H, Vargas C de, Iudicone D, Bowler C, Wincker P. 2018. A global ocean atlas of eukaryotic genes. Nature Communications 9:373.

110. Keeling PJ, Burki F, Wilcox HM, Allam B, Allen EE, Amaral-Zettler LA, Armbrust EV, Archibald JM, Bharti AK, Bell CJ, Beszteri B, Bidle KD, Cameron CT, Campbell L, Caron DA, Cattolico RA, Collier JL, Coyne K, Davy SK, Deschamps P, Dyhrman ST, Edvardsen B, Gates RD, Gobler CJ, Greenwood SJ, Guida SM, Jacobi JL, Jakobsen KS, James ER, Jenkins B, John U, Johnson MD, Juhl AR, Kamp A, Katz LA, Kiene R, Kudryavtsev A, Leander BS, Lin S, Lovejoy C, Lynn D, Marchetti A, McManus G, Nedelcu AM, Menden-Deuer S, Miceli C, Mock T, Montresor M, Moran MA, Murray S, Nadathur G, Nagai S, Ngam PB, Palenik B, Pawlowski J, Petroni G, Piganeau G, Posewitz MC, Rengefors K, Romano G, Rumpho ME, Rynearson T, Schilling KB, Schroeder DC, Simpson AGB, Slamovits CH, Smith DR, Smith GJ, Smith SR, Sosik HM, Stief P, Theriot E, Twary SN, Umale PE, Vaulot D, Wawrik B, Wheeler GL, Wilson WH, Xu Y, Zingone A, Worden AZ. 2014. The Marine Microbial Eukaryote Transcriptome Sequencing Project (MMETSP): Illuminating the Functional Diversity of Eukaryotic Life in the Oceans through Transcriptome Sequencing. PLOS Biology 12:e1001889.

111. Buchfink B, Xie C, Huson DH. 2015. Fast and sensitive protein alignment using DIAMOND. Nat Methods 12:59–60.

# Figure legends

**FIG 1** PkV RF01 morphology and reduced viral infectivity under chloroform treatment. (A) Screen shot of a cryo-electron tomogram of a PkV RF01 virion. (B) Composite image of 61 cryo-electron tomograms (–60 to 60°, imaged every 2°). Purple, capsid; green, inner membrane consisting of multiple irregular, convoluted membranes; blue, internal rod-shaped core filled with dense material. The full set of records is available on GitHub (see Data availability section). Scale bar, 100 nm. (C) Reduction of PkV RF01 infectivity with chloroform. Experiments were set up in triplicate, and host cells were counted by flow cytometry. Chloroform-treated PkV RF01 was added to exponentially growing He UiO028 cells in a 1:10 volume ratio. Controls were He UiO028 cells incubated with chloroform-treated medium (Control A), untreated PkV RF01 (Control B), and untreated medium (Control C). SDs are indicated with error bars.

**FIG 2** Structure and gene taxonomic composition of the PkV RF01 genome sequence. (A) Rhizome and genomic features of the PkV RF01 genome. As illustrated by the rhizome (inner part of the figure), ORFans comprise the largest set of PkV RF01 genes, and a substantial portion (15%) have their best BLAST hits (in UniRef90) against "*Mimiviridae*." Colors indicate taxonomic origin. Intergenic regions are white. Percentage hits per taxonomic group higher than 5% of total genes are indicated. In the outermost ring, rectangles indicate the positions of glycosyltransferases (white), lipid-related enzymes (black), and succinate dehydrogenase genes (red), and the numbers correspond to *Mimiviridae* key enzymes (1 and 3: DNA-directed RNA polymerase II subunits 1 and 2, respectively; 2: DNA mismatch repair protein MutS7; 4: Packaging ATPase; 5: VLTF3, 6: Major capsid protein; 7: Eukaryotic translation

initiation factor 4E; 8: Asparagine synthase; 9: DNA polymerase family B). The ring adjacent to the outermost ring shows GC skew over a 10-KB window. (B) Taxonomic breakdown of 180 genes with best hits to virus genes. Mega, Megavirinae; AaV, Aureococcus anophagefferens virus; TetV, Tetraselmis virus 1; PoV, Pyramimonas orientalis virus.

**FIG 3** Phylogenetic evidence for PkV RF01 as a distant relative of "Mesomimivirinae." (A) Bayesian phylogenetic tree of NCLDVs reconstructed from a concatenated alignment of five core nucleocytoplasmic virus orthologous genes. Values at branches are posterior probabilities support. The tree was rooted using *Poxviridae* as outgroup. The scale bar indicates substitutions per site. (B) Maximum likelihood phylogenetic tree of cellular and NCLDV DNA-directed RNA polymerase subunit beta (RPB2). Values at branches are Shimodaira-Hasegawa-like local support.

**FIG 4** COG functional distribution of 339 proteins encoded by PkV RF01.

**FIG 5** Comparative COG functional distribution among Mimiviridae members. COG sequences were automatically searched against the proteomes of each virus using BLASTP with an E-value of 1 × 10−5 as the significant similarity threshold.

**FIG 6** Bayesian phylogenetic trees of two viral amino-acyl tRNA synthetases and their cellular homologs. (A) Isoleucine tRNA synthases. (B) Aspartyl tRNA synthetases. Branches supported by posterior probability (PP) values >70% are indicated by circles whose diameters are proportional to the PP value.

**FIG 7** Genes in PkV RF01 predicted to encode enzymes of oxidative phosphorylation and β-oxidation pathways. (A) Gene organization in the succinate dehydrogenase-containing region. (B) Schematic representation of the canonical enzymatic complex II in the mitochondrial membrane. (C) Location of succinate dehydrogenase in the TCA cycle and electron transport chain as known in plants and a schematic reconstruction of the PkV RF01-encoded β-oxidation metabolic pathway.

**FIG 8** The viral SDHA gene is transcribed during infection. Gels of PCR and RT-PCR in combination with a TURBO DNA-free kit. Samples were taken 24, 72, and 96 h after infection. (A) PCR with *vSDHA*-specific primers was used to check for the presence of genomic DNA after RNA isolation treated with 1x and 2x DNAse, in the upper and lower panels respectively. P, positive control (PKV RF01 genomic DNA); N, negative control ($sdH_20$). (B) RT-PCR of RNA samples using *vSDHA*-specific primers. M, DNA marker (MassRuler DNA Ladder Mix, Thermo Fisher, 80 to 10,000 bp).

**FIG 9** PCR optimization and confirmation of the SDHA gene in the PkV RF01 genome. (A–B) Results of PCR with SDHA primers using genomic PkV RF01 DNA (A) and genomic He UiO028 DNA (B) as templates. Lanes 1 and 9, DNA ladder; 2–7, optimization of the PCR annealing temperature from 55°C (2) to 60°C (7); 8, negative control (sdH2O).

**FIG 10** PCR and RT-PCR optimization using an internal control gene (mcp). PCR and RT-PCR were carried out after removal of genomic DNA using a TURBO DNA-free kit. Samples were taken 24, 72, and 96 h after infection. Two different

protocols, both provided in the TURBO DNA-free kit manual, were used to optimize the reactions. (A) PCR check for the presence of genomic DNA after RNA isolation treated with 1x and 2x DNAse, in the upper and lower panels respectively. P, positive control (PkV RF01 genomic DNA); N, negative control (sdH20). (B) Result of RT-PCR of samples harvested 24, 72 and 96 h post infection. M, DNA marker (MassRuler DNA Ladder Mix, Thermo Fisher, 80 to 10,000 bp).

**FIG 11** Origin of PkV RF01 SDHA and SDHB and their most similar homologs in *Tara* Oceans metagenomes. (A) Taxonomy of genes predicted in *Tara* Oceans metagenome assembled-genome fragments encoding the 50 SDHAs and SDHBs most similar to PkV RF01 genes (for genome fragments having at least five predicted genes). (B and C) Phylogenetic trees of viral and cellular SDHAs (B) and SDHBs (C). Clades in green contain PkV RF01 SDHA or SDHB and their 50 most similar hits identified in *Tara* Oceans metagenomes (predicted to be *Mimiviridae* homologs from A). Red, eukaryotic phyla; black, unclassified eukaryotes. Trees are rooted with Proteobacteria and Firmicutes homologs (not shown). Circles indicate branches with posterior probability support ≥ 50%.

**FIG 12** Comparative distribution of glycosyltransferase domains among viruses.

# Tables

**TABLE 1** Infection parameters of *Prymnesium kappa* viruses RF01 and RF02 and *Haptolina ericina* virus RF02.

| Viral species and hosts | Infectious progeny/mL (MPN) | Host cells/mL (FCM)[a] | Total VLP/mL (FCM) | Burst size (VLP)[b] | Infectivity (%)[c] | Infectious particles in a burst[d] |
|---|---|---|---|---|---|---|
| PkV RF01 (He UiO028) | $2.9\times10^{6}$ (± 0.2) | $4.9\times10^{5}$ | $1.8\times10^{8}$ (±0.9) | 363 | 2 | 6 |
| PkV RF02 (Pk RCC3423) | $2.2\times10^{8}$ (± 0.2) | $4.6\times10^{5}$ | $5.0\times10^{8}$ (±0.1) | 1093 | 44 | 483 |
| HeV RF02 (He UiO028) | $5.8\times10^{7}$ (±0.2) | $4.9\times10^{5}$ | $4.4\times10^{8}$ (±0.0) | 907 | 13 | 119 |

VLP, virus-like particle; MPN, most probable number; FCM, flow cytometry.
[a]Measurement performed in duplicates
[b]The number of viral particles released from each host cell, estimated from the total number of host cells pre-infection and the total number of VLPs produced during the infection cycle.
[c]Estimated as the percentage of infectious progeny of all VLPs produced during the infection cycle.
[d]Number of infectious particles released per host cell.

**TABLE 2** Gene related to lipid metabolism.

| ORF | Annotation | KEGG orthology | Pathway |
|---|---|---|---|
| 30 | 2,4-dienoyl-CoA reductase, mitochondrial [EC:1.3.1.34] | K13236 | Beta oxidation |
| 33 | Putative CoA-transferase | NS | Beta oxidation |
| 121 | glycerophosphoryl diester phosphodiesterase | K01126 | Glycerophospholipids metabolisms |
| 138 | Fatty acid synthase (FASN) | K00665 | Fatty acid biosynthesis |
| 142 | Long-chain-fatty-acid--CoA ligase ACSBG [EC:6.2.1.3] | K15013 | Fatty acid degradation /biosynthesis / Beta Oxidation |
| 175 | Acetyl-CoA carboxylase / biotin carboxylase 1 [EC:6.4.1.2 6.3.4.14 2.1.3.15] | K11262 | Fatty acid biosynthesis |
| 236 | Glutaryl-CoA dehydrogenase [EC:1.3.8.6] | K00252 | Fatty acid degradation |
| 293 | Lysophospholipase like | NS | NS |
| 357 | Lysophospholipase like | NS | NS |
| 386 | Triacylglycerol lipase [EC:3.1.1.3] | K01046 | Glycerolipid metabolism |
| 481 | Lipase like | NS | NS |
| 635 | Lipase-like | NS | NS |
| 653 | Lipase-like | NS | NS |
| 690 | Lipase-like | NS | NS |
| 774 | Lysophospholipid Acyltransferases [EC:2.3.1.22] | K14457 | Glycerolipid metabolism |
| 694 | Lipase esterase (Carbohydrate esterase CE10) | NS | NS |
| 695 | Lipase esterase (Carbohydrate esterase CE10) | NS | NS |
| 886 | Stearoyl-CoA desaturase (Delta-9 desaturase) [EC:1.14.19.1] | K00507 | Biosynthesis of unsaturated fatty acids |
| 902 | Fatty acid synthase (FASN) | K00665 | Fatty acid biosynthesis |

| | | | |
|---|---|---|---|
| 904 | Long-chain-fatty-acid--CoA ligase ACSBG [EC:6.2.1.3] | K15013 | Fatty acid degradation /biosynthesis / Beta Oxidation |
| 1016 | Cyclopropane-fatty-acyl-phospholipid synthase [EC:2.1.1.79] | k00574 | NS |
| 1046 | Acyl-CoA dehydrogenase | K06445 | Fatty acid degradation / Beta oxidation |

**TABLE 3** Forward and reverse PCR primers for amplification of vSDHA and MCP

| Primer name | Sequence (5´- 3´) | PCR product (bp) |
|---|---|---|
| vSDHA-F1 | ATGTGCCGAGAAGCTCCTAA | 154 |
| vSDHA-R1 | CTGCACAGGCTGTTCGATAA | |
| PkV-RF01-MCP-F | GATGAACCTTGCCCACAACT | 256 |
| PkV-RF01-MCP-F | GTGCATGGTACGTTTTCGTG | |

# Figure 1

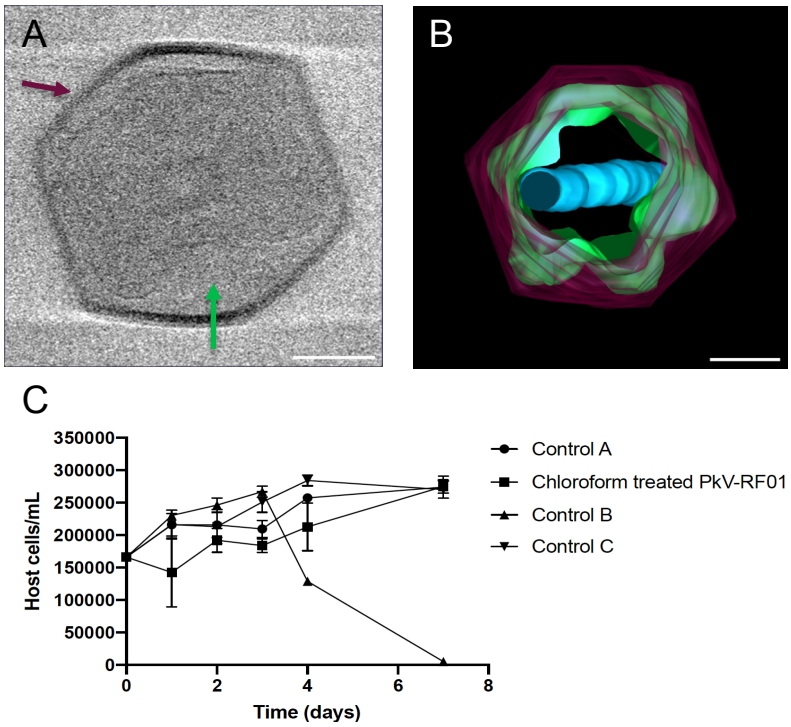
A
B
C
Host cells/mL
350000
300000
250000
200000
150000
100000
50000
0
0
2
4
6
8
Time (days)
Control A
Chloroform treated PkV-RF01
Control B
Control C

Figure 2

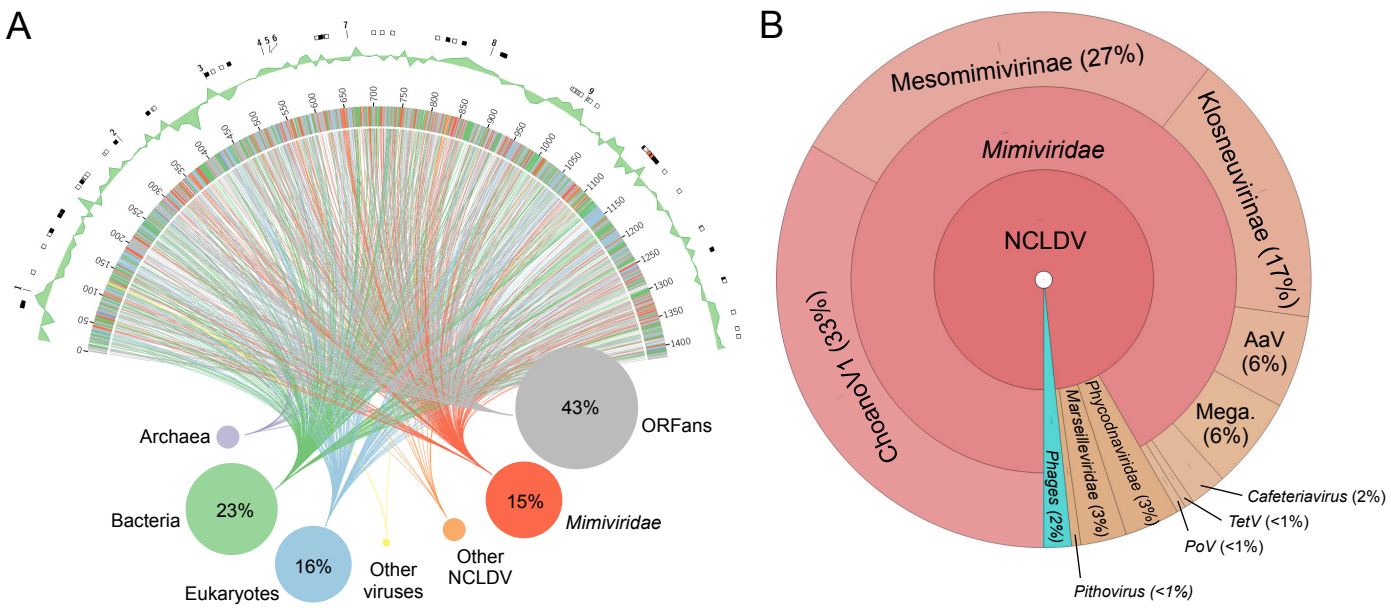
A
Archaea
Bacteria
23%
Eukaryotes
16%
Other viruses
Other NCLDV
15%
Mimiviridae
43%
ORFans
B
Mesomimivirinae (27%)
Mimiviridae
NCLDV
Klosneuvirinae (17%)
AaV (6%)
Mega. (6%)
Phycodnaviridae (3%)
Marseilleviridae (3%)
Phages (2%)
Cafeteriavirus (2%)
TetV (<1%)
PoV (<1%)
Pithovirus (<1%)
Choanovi (33%)

# Figure 3

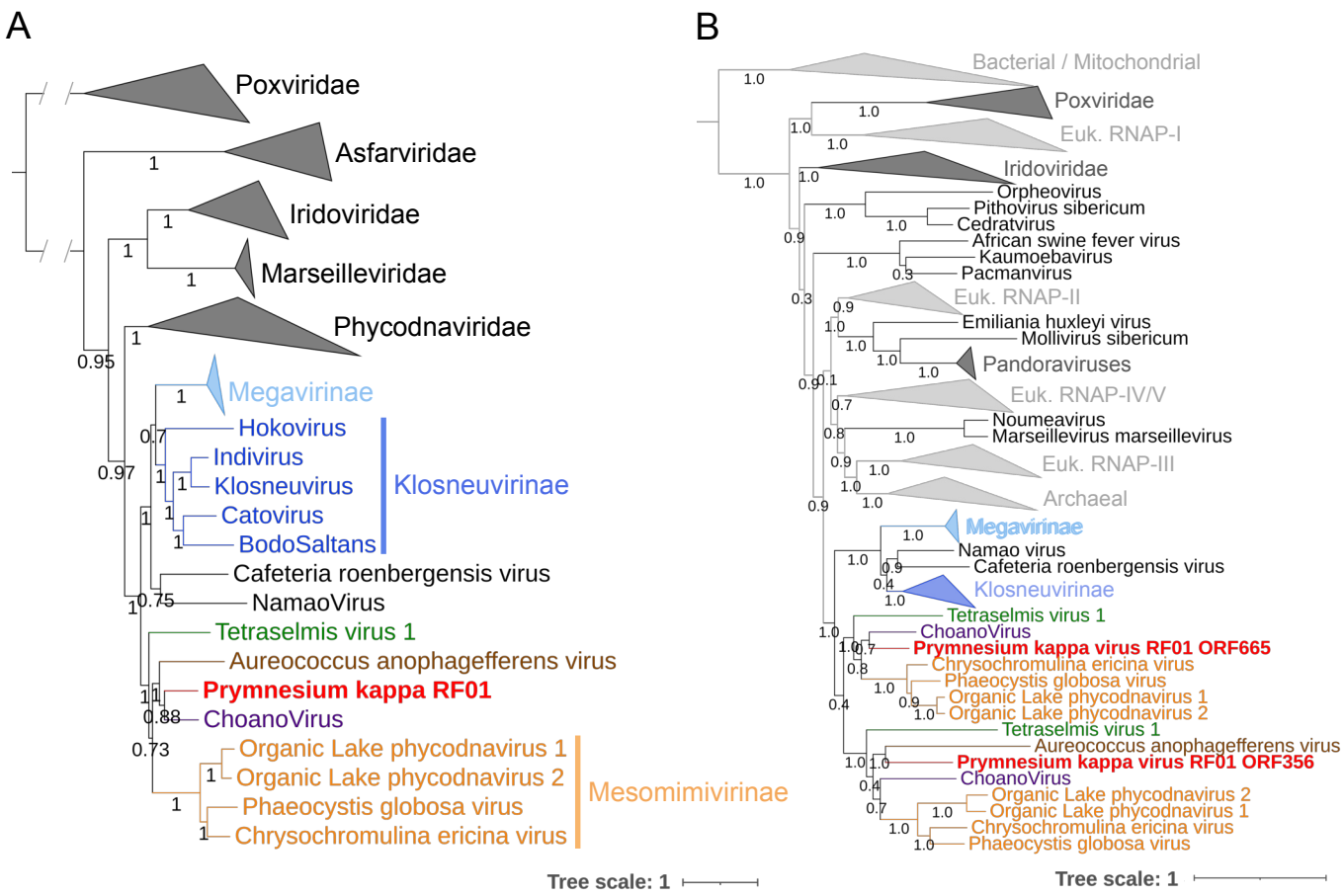
A
Poxviridae
Asfarviridae
Iridoviridae
Marseilleviridae
Phycodnaviridae
Megavirinae
Hokovirus
Indivirus
Klosneuvirus
Catovirus
BodoSaltans
Klosneuvirinae
Cafeteria roenbergensis virus
NamaoVirus
Tetraselmis virus 1
Aureococcus anophagefferens virus
Prymnesium kappa RF01
ChoanoVirus
Organic Lake phycodnavirus 1
Organic Lake phycodnavirus 2
Phaeocystis globosa virus
Chrysochromulina ericina virus
Mesomimivirinae
Tree scale: 1
B
Bacterial / Mitochondrial
Poxviridae
Euk. RNAP-I
Iridoviridae
Orpheovirus
Pithovirus sibericum
Cedratvirus
African swine fever virus
Kaumoebavirus
Pacmanvirus
Euk. RNAP-II
Emiliania huxleyi virus
Mollivirus sibericum
Pandoraviruses
Euk. RNAP-IV/V
Noumeavirus
Marseillevirus marseillevirus
Euk. RNAP-III
Archaeal
Megavirinae
Namao virus
Cafeteria roenbergensis virus
Klosneuvirinae
Tetraselmis virus 1
ChoanoVirus
Prymnesium kappa virus RF01 ORF665
Chrysochromulina ericina virus
Phaeocystis globosa virus
Organic Lake phycodnavirus 1
Organic Lake phycodnavirus 2
Tetraselmis virus 1
Aureococcus anophagefferens virus
Prymnesium kappa virus RF01 ORF356
ChoanoVirus
Organic Lake phycodnavirus 2
Organic Lake phycodnavirus 1
Chrysochromulina ericina virus
Phaeocystis globosa virus
Tree scale: 1

# Figure 4

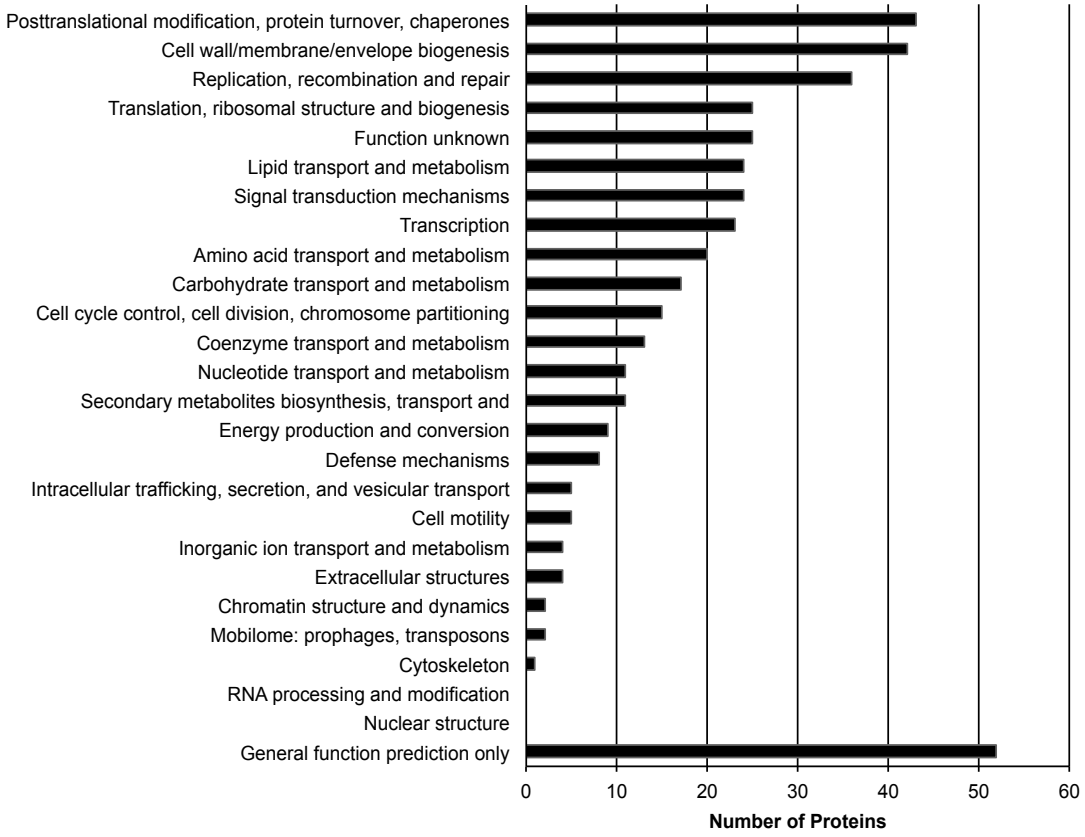
Posttranslational modification, protein turnover, chaperones
Cell wall/membrane/envelope biogenesis
Replication, recombination and repair
Translation, ribosomal structure and biogenesis
Function unknown
Lipid transport and metabolism
Signal transduction mechanisms
Transcription
Amino acid transport and metabolism
Carbohydrate transport and metabolism
Cell cycle control, cell division, chromosome partitioning
Coenzyme transport and metabolism
Nucleotide transport and metabolism
Secondary metabolites biosynthesis, transport and
Energy production and conversion
Defense mechanisms
Intracellular trafficking, secretion, and vesicular transport
Cell motility
Inorganic ion transport and metabolism
Extracellular structures
Chromatin structure and dynamics
Mobilome: prophages, transposons
Cytoskeleton
RNA processing and modification
Nuclear structure
General function prediction only
0
10
20
30
40
50
60
Number of Proteins

Figure 5

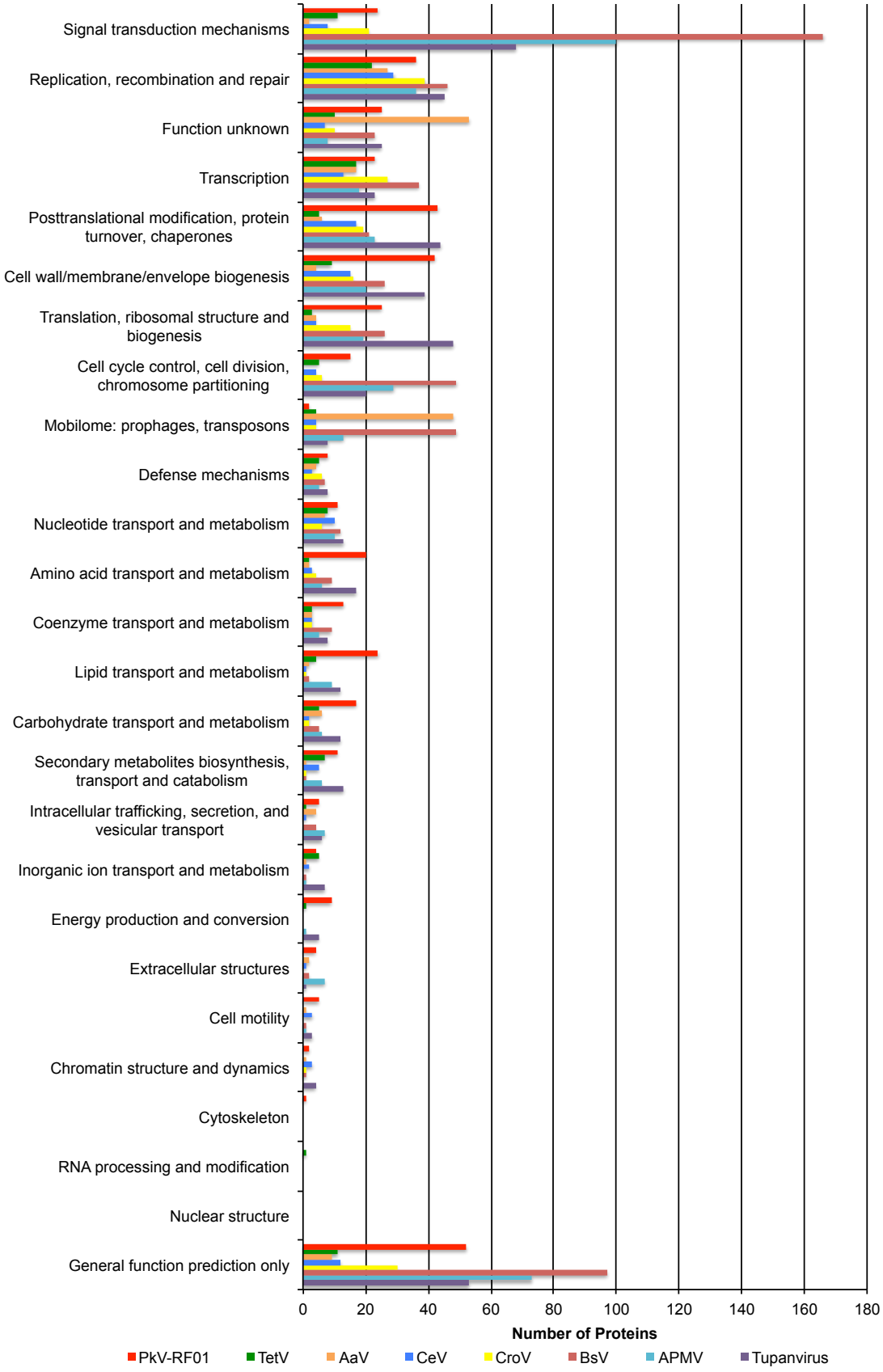
Signal transduction mechanisms
Replication, recombination and repair
Function unknown
Transcription
Posttranslational modification, protein turnover, chaperones
Cell wall/membrane/envelope biogenesis
Translation, ribosomal structure and biogenesis
Cell cycle control, cell division, chromosome partitioning
Mobilome: prophages, transposons
Defense mechanisms
Nucleotide transport and metabolism
Amino acid transport and metabolism
Coenzyme transport and metabolism
Lipid transport and metabolism
Carbohydrate transport and metabolism
Secondary metabolites biosynthesis, transport and catabolism
Intracellular trafficking, secretion, and vesicular transport
Inorganic ion transport and metabolism
Energy production and conversion
Extracellular structures
Cell motility
Chromatin structure and dynamics
Cytoskeleton
RNA processing and modification
Nuclear structure
General function prediction only
0
20
40
60
80
100
120
140
160
180
Number of Proteins
PkV-RF01
TetV
AaV
CeV
CroV
BsV
APMV
Tupanvirus

Figure 6

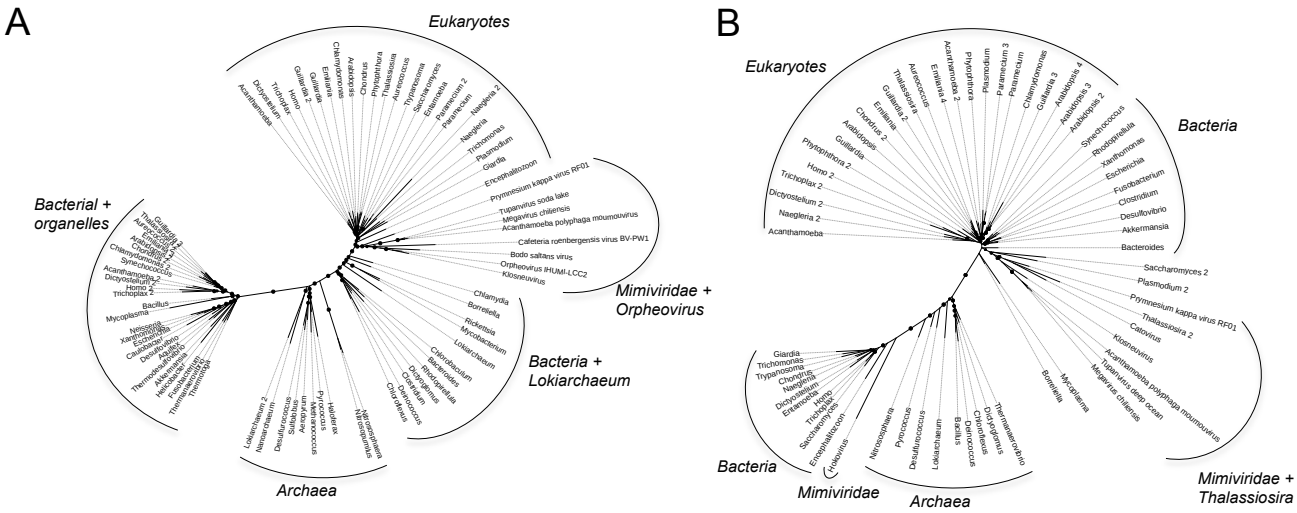
A
Eukaryotes
Bacterial + organelles
Mimiviridae + Orpheovirus
Bacteria + Lokiarchaeum
Archaea
B
Eukaryotes
Bacteria
Bacteria
Mimiviridae
Archaea
Mimiviridae + Thalassiosira

# Figure 7

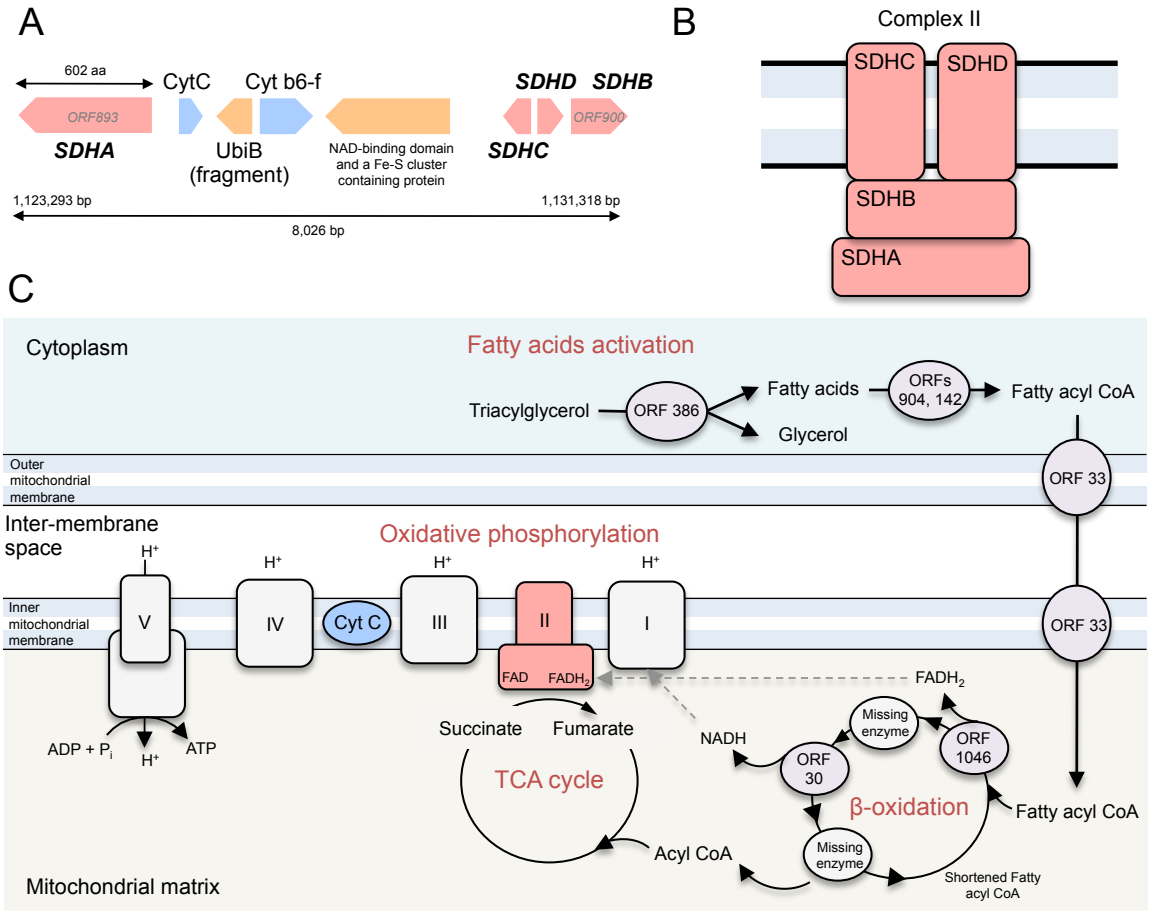
A
602 aa
CytC
Cyt b6-f
SDHD
SDHB
ORF893
ORF900
SDHA
UbiB
(fragment)
NAD-binding domain
and a Fe-S cluster
containing protein
SDHC
1,123,293 bp
1,131,318 bp
8,026 bp
B
Complex II
SDHC
SDHD
SDHB
SDHA
C
Cytoplasm
Fatty acids activation
Triacylglycerol
ORF 386
Fatty acids
Glycerol
ORFs
904, 142
Fatty acyl CoA
ORF 33
Outer
mitochondrial
membrane
Inter-membrane
space
Oxidative phosphorylation
H+
V
IV
Cyt C
III
II
I
Inner
mitochondrial
membrane
FAD
FADH2
ADP + Pi
ATP
Succinate
Fumarate
TCA cycle
NADH
Missing
enzyme
ORF
30
ORF
1046
β-oxidation
Acyl CoA
Shortened Fatty
acyl CoA
Mitochondrial matrix

Figure 8

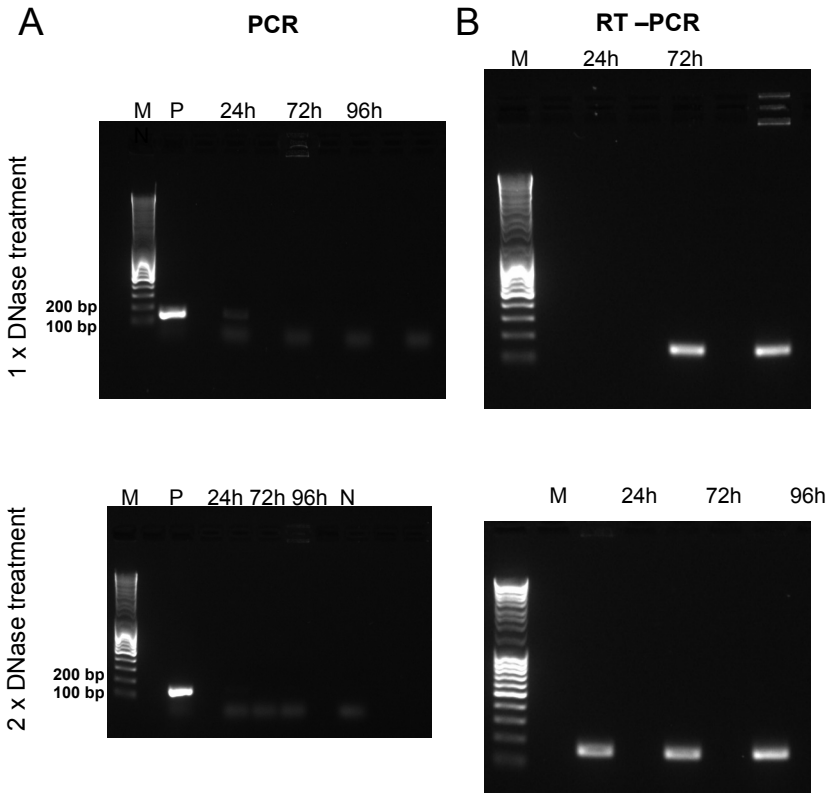
A
PCR
B
RT –PCR
M P 24h 72h 96h
N
M 24h 72h
1 x DNase treatment
200 bp
100 bp
M P 24h 72h 96h N
M 24h 72h 96h
2 x DNase treatment
200 bp
100 bp

Figure 9

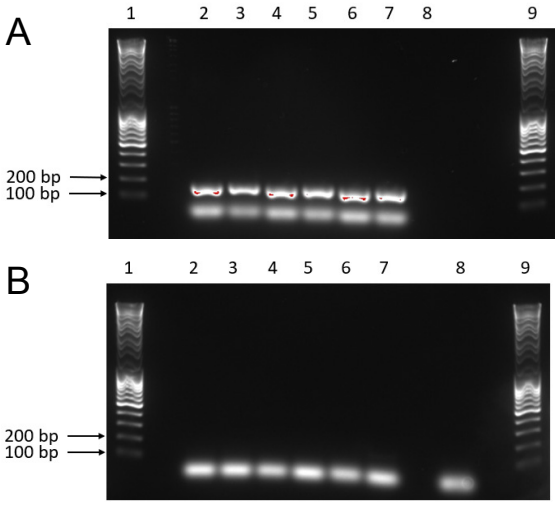

Figure 10

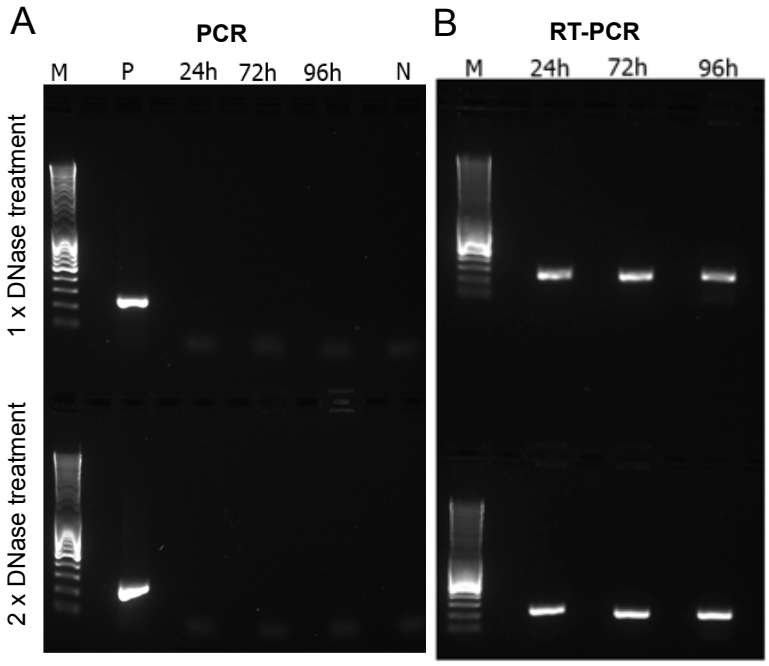
A
PCR
M
P
24h
72h
96h
N
1 x DNase treatment
2 x DNase treatment
B
RT-PCR
M
24h
72h
96h

# Figure 11

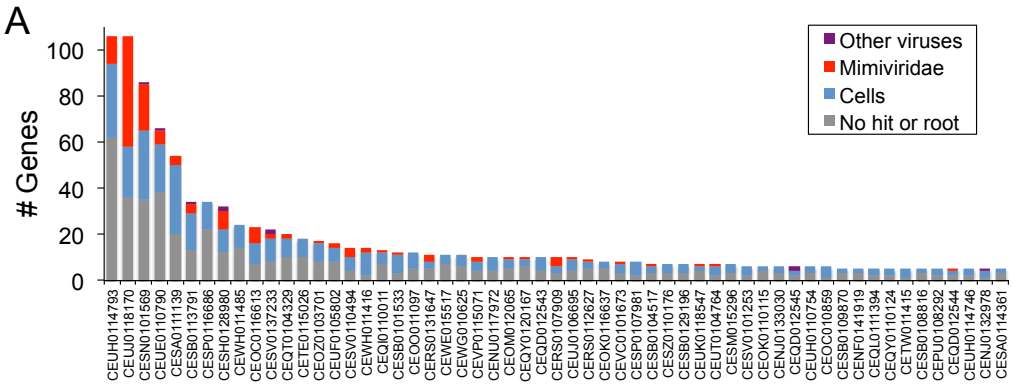
A
# Genes
100
80
60
40
20
0
Other viruses
Mimiviridae
Cells
No hit or root
CEUH0114793
CEUJ0118170
CESN0101569
CEUE0110790
CESA0111139
CESB0113791
CESP0116686
CESH0128980
CEWH0111485
CEOC0116613
CESV0137233
CEQT0104329
CETE0115026
CEQZ0103701
CEUF0105802
CESV0110494
CEWH0111416
CEQI0110011
CESB0101533
CEOO0111097
CERS0131647
CEWE0115517
CEWG0110625
CEVP0115071
CENU0117972
CEOM0112065
CEQY0120167
CEQD0012543
CERS0107909
CEUJ0106695
CERS0112627
CEOK0116637
CEVC0101673
CESP0107981
CESB0104517
CESZ0110176
CESB0129196
CEUK0118547
CEUT0104764
CESM0115296
CESV0101253
CEOK0110115
CENJ0133030
CEQD0012545
CEUH0110754
CEOC0110859
CESB0109870
CENF0141919
CEQL0111394
CEQY0110124
CETW0111415
CESB0108816
CEPU0108292
CEQD0012544
CEUH0114746
CENJ0132978
CESA0114361

B

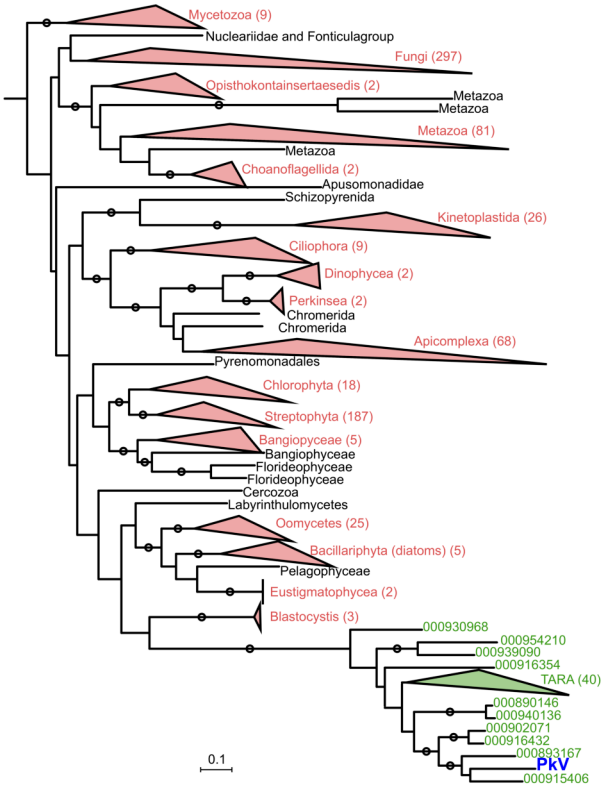
Mycetozoa (9)
Nucleariidae and Fonticulagroup
Fungi (297)
Opisthokontainsertaesedis (2)
Metazoa
Metazoa
Metazoa (81)
Metazoa
Choanoflagellida (2)
Apusomonadidae
Schizopyrenida
Kinetoplastida (26)
Ciliophora (9)
Dinophycea (2)
Perkinsea (2)
Chromerida
Chromerida
Apicomplexa (68)
Pyrenomonadales
Chlorophyta (18)
Streptophyta (187)
Bangiopyceae (5)
Bangiophyceae
Florideophyceae
Florideophyceae
Cercozoa
Labyrinthulomycetes
Oomycetes (25)
Bacillariphyta (diatoms) (5)
Pelagophyceae
Eustigmatophycea (2)
Blastocystis (3)
000930968
000954210
000939090
000916354
TARA (40)
000890146
000940136
000902071
000916432
000893167
PkV
000915406
0.1

C

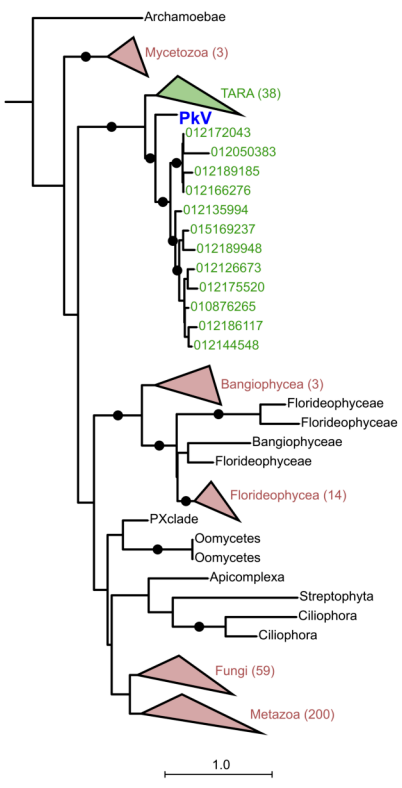
Archamoebae
Mycetozoa (3)
TARA (38)
PkV
012172043
012050383
012189185
012166276
012135994
015169237
012189948
012126673
012175520
010876265
012186117
012144548
Bangiophycea (3)
Florideophyceae
Florideophyceae
Bangiophyceae
Florideophyceae
Florideophycea (14)
PXclade
Oomycetes
Oomycetes
Apicomplexa
Streptophyta
Ciliophora
Ciliophora
Fungi (59)
Metazoa (200)
1.0

Figure 12

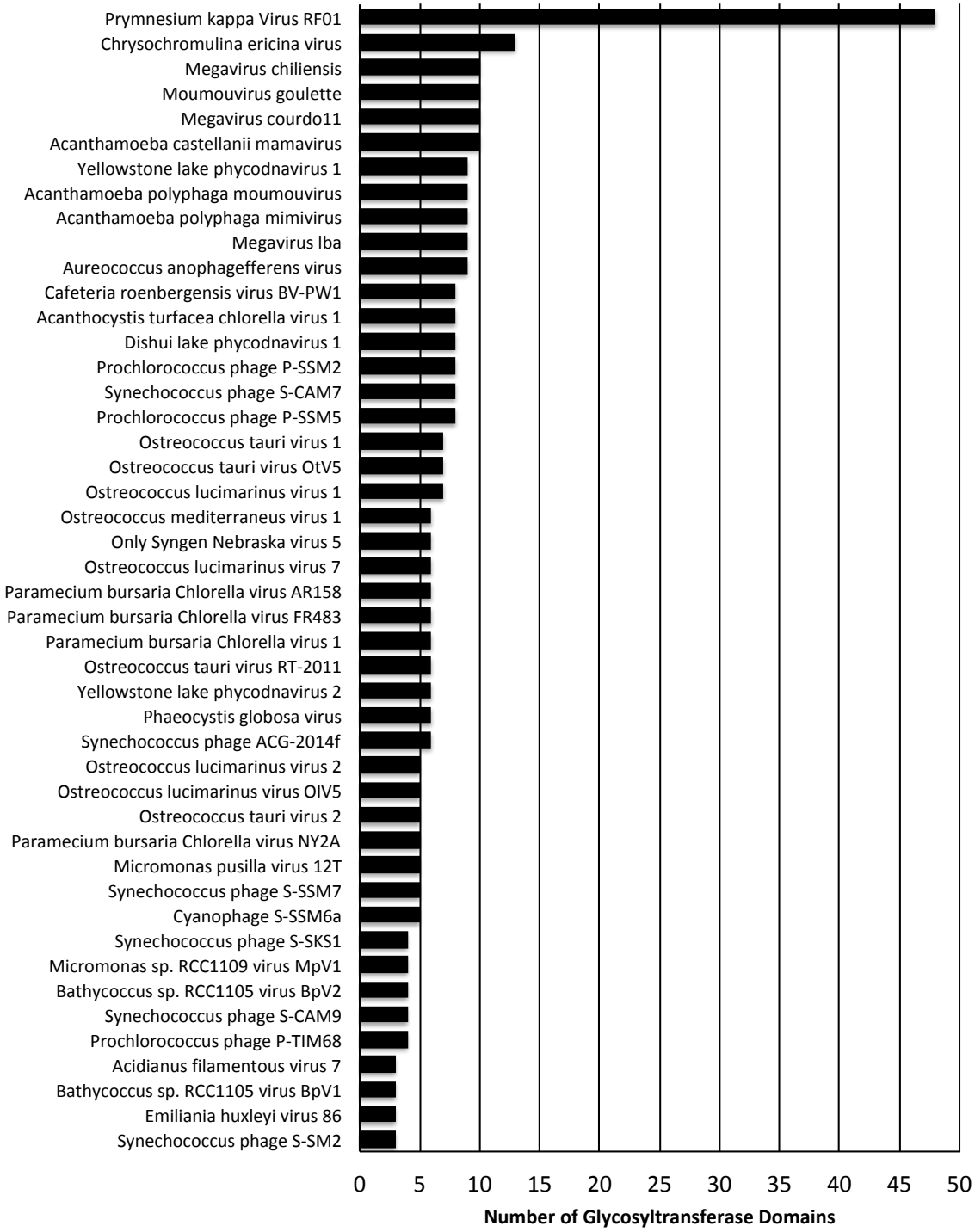
Prymnesium kappa Virus RF01
Chrysochromulina ericina virus
Megavirus chiliensis
Moumouvirus goulette
Megavirus courdo11
Acanthamoeba castellanii mamavirus
Yellowstone lake phycodnavirus 1
Acanthamoeba polyphaga moumouvirus
Acanthamoeba polyphaga mimivirus
Megavirus lba
Aureococcus anophagefferens virus
Cafeteria roenbergensis virus BV-PW1
Acanthocystis turfacea chlorella virus 1
Dishui lake phycodnavirus 1
Prochlorococcus phage P-SSM2
Synechococcus phage S-CAM7
Prochlorococcus phage P-SSM5
Ostreococcus tauri virus 1
Ostreococcus tauri virus OtV5
Ostreococcus lucimarinus virus 1
Ostreococcus mediterraneus virus 1
Only Syngen Nebraska virus 5
Ostreococcus lucimarinus virus 7
Paramecium bursaria Chlorella virus AR158
Paramecium bursaria Chlorella virus FR483
Paramecium bursaria Chlorella virus 1
Ostreococcus tauri virus RT-2011
Yellowstone lake phycodnavirus 2
Phaeocystis globosa virus
Synechococcus phage ACG-2014f
Ostreococcus lucimarinus virus 2
Ostreococcus lucimarinus virus OlV5
Ostreococcus tauri virus 2
Paramecium bursaria Chlorella virus NY2A
Micromonas pusilla virus 12T
Synechococcus phage S-SSM7
Cyanophage S-SSM6a
Synechococcus phage S-SKS1
Micromonas sp. RCC1109 virus MpV1
Bathycoccus sp. RCC1105 virus BpV2
Synechococcus phage S-CAM9
Prochlorococcus phage P-TIM68
Acidianus filamentous virus 7
Bathycoccus sp. RCC1105 virus BpV1
Emiliania huxleyi virus 86
Synechococcus phage S-SM2
0
5
10
15
20
25
30
35
40
45
50
Number of Glycosyltransferase Domains